Received 21 February 2020; revised 12 March 2020; accepted 19 March 2020.
Date of publication 23 March 2020; date of current version 17 April 2020.

Digital Object Identifier 10.1109/OJCOMS.2020.2982770

Sum of Fisher-Snedecor $\mathcal{F}$ Random Variables and Its Applications

HONGYANG DU[1], JIAYI ZHANG[1] (Member, IEEE), JULIAN CHENG[2] (Senior Member, IEEE), AND BO AI[3] (Senior Member, IEEE)

[1]School of Electronic and Information Engineering, Beijing Jiaotong University, Beijing 100044, China

[2]School of Engineering, University of British Columbia, Kelowna, BC V1V 1V7, Canada

[3]State Key Laboratory of Rail Traffic Control and Safety, Beijing Jiaotong University, Beijing 100044, China

CORRESPONDING AUTHOR: J. ZHANG (e-mail: jiayizhang@bjtu.edu.cn)

This work was supported in part by the National Key Research and Development Program under Grant 2016YFE0200900, in part by the Royal Society Newton Advanced Fellowship under Grant NA191006, in part by the State Key Laboratory of Rail Traffic Control and Safety under Grant RCS2018ZZ007 and Grant RCS2019ZZ007, in part by the National Natural Science Foundation of China under Grant 61971027, Grant U1834210, Grant 61961130391, Grant 61625106, and Grant 61725101, in part by the Beijing Natural Science Foundation under Grant 4182049 and Grant L171005, in part by the Engineering Research Center of Mobile Communications, Ministry of Education under Grant CQUPT-MCT-201804, in part by the Science and Technology Key Project of Guangdong Province, China, under Grant 2019B010157001, in part by the National Training Program of Innovation and Entrepreneurship for Undergraduates under Grant 202010004002, and in part by ZTE Corporation.

ABSTRACT The statistical characterization of a sum of random variables (RVs) is useful for investigating the performance of wireless communication systems. We derive exact closed-form expressions for the probability density function (PDF) and cumulative distribution function (CDF) of a sum of independent but not identically distributed (i.n.i.d.) Fisher-Snedecor $\mathcal{F}$ RVs. Both PDF and CDF are expressed in terms of the multivariate Fox's H-function. Besides, a simple and accurate approximation to the sum of i.n.i.d. Fisher-Snedecor $\mathcal{F}$ variates is presented using the moment matching method. The obtained PDF and CDF are used to evaluate the performance of wireless communication applications including the outage probability, the effective capacity, and the channel capacities under four different adaptive transmission strategies. Moreover, the corresponding approximate expressions are obtained to provide useful insights for the design and deployment of wireless communication systems. In addition, we derive simple asymptotic expressions for the proposed mathematical analysis in the high signal-to-noise ratio regime. Finally, the numerical results demonstrate the accuracy of the derived expressions.

INDEX TERMS Channel capacity, effective capacity, Fisher-Snedecor $\mathcal{F}$-distribution, sum of random variables.

I. INTRODUCTION

RECENTLY, the Fisher-Snedecor $\mathcal{F}$ distribution was proposed [1] as a tractable fading model to describe the combined effects of shadowing and multipath fading in future wireless communications. This distribution can be reduced to some common fading models, such as Nakagami-m, Rician, and Rayleigh fading channels [2]–[5]. Furthermore, it is found [1] that the $\mathcal{F}$ distribution can provide a better fit to the experimental data obtained for device-to-device (D2D) and wearable communication links, especially at 5.8 GHz, as compared with the well established generalized-K (GK) distribution. In addition, its probability density function (PDF) consists of only elementary functions and it leads to more tractable analysis than the GK model [1]. Due to its promising properties, the performance of digital communication systems over $\mathcal{F}$ distributed fading channels has been analyzed in [6]–[11] and the references therein.

The sum of random variables (RVs) has a wide range of important applications in the performance analysis of wireless communication systems. For example, to enhance the quality of the received signal, maximal-ratio combining (MRC) can be deployed at the receiver to maximize the combiner output signal-to-noise ratio (SNR) [12]. The MRC

receiver operating over different fading channels has been extensively studied [13]–[18]. Furthermore, approximations to distributions of sum of RVs have been also intensively studied [19]–[22], and several methods have been adopted to simplify the performance analysis.

The PDF and cumulative distribution function (CDF) of the sum of Fisher-Snedecor $\mathcal{F}$ RVs have been derived in terms of Lauricella multivariate hypergeometric function [23]. However, there are some several typographical errors in the PDF and CDF expressions for both independent but not identically distributed (i.n.i.d.) case and independent and identically distributed (i.i.d.) case that are respectively given as [23, eq. (4)], [23, eq. (5)], [23, eq. (8)] and [23, eq. (9)]. Furthermore, these analytical results are difficult to be used in the performance analysis of MRC systems over Fisher-Snedecor $\mathcal{F}$ fading channels due to the complex Lauricella multivariate hypergeometric function. Moreover, the authors in [23] obtained outage probability (OP) and outage capacity expressions involving L-fold Mellin-Barnes type contour integral, where L is the number of diversity branches. These results cannot be calculated efficiently because the integration will be more difficult to converge as L increases. Thus, the insights into the system performance are limited.

In addition, the authors in [24] presented exact closed-form expressions for PDF and CDF of the sum of i.n.i.d. H-function RVs. Thus, the distribution of the sum of Fisher-Snedecor $\mathcal{F}$ RVs can be derived as a special case. However, the calculation of multivariate Fox's H-function proposed in [24] is time-consuming because when its multivariate Fox's H-function is written in the form of Merlin-Barnes integral, we observe that it has L integral variables in the same gamma function. Besides, the statistical characterization is challenging, if not impossible, to derive the important performance metrics. For the i.i.d. case, the difficulty of calculation will not be reduced either.

To fill this gap, we re-investigate the statistical characterization of the sum of i.n.i.d. Fisher-Snedecor $\mathcal{F}$ RVs and leverage the PDF and CDF expressions to analyze the performance of the MRC receiver in terms of outage probability, channel capacity, and effective capacity. The main contributions of this paper are summarized as follows:

- We derive exact closed-form expressions for the PDF and CDF of the sum of i.n.i.d. Fisher-Snedecor $\mathcal{F}$ RVs in terms of a new form of multivariate Fox's H-function, which can be efficiently programmed in standard software packages (e.g., MATLAB, Mathematica and Python) [25]–[28]. In addition, when the multivariate Fox's H-function is written in the form of Merlin-Barnes integral, there are at most two integral variables in the same gamma function, so the calculation process is efficient.
- We introduce a paradigm based on the moment matching method to obtain a simple approximation to the sum of Fisher-Snedecor $\mathcal{F}$ RVs using another single $\mathcal{F}$ RV. To improve the accuracy of the approximation, we propose an adjustment factor to modify the error in the lower and upper tail regions. The approximated expression is easier to evaluate. We employ the Kolmogorov-Smirnov (KS) goodness-of-fit test to show that the single $\mathcal{F}$ distribution is a highly accurate approximation to the sum of $\mathcal{F}$ RVs.
- We derive novel analytical expressions for important performance metrics, namely the OP, the effective capacity, and the channel capacities under four different adaptive transmission schemes, including optimal rate adaptation with constant transmit power (ORA), simultaneous optimal power and rate adaptation (OPRA), channel inversion with fixed rate (CIFR) and truncated channel inversion with fixed rate (TIFR). Moreover, the final value theorem is used to avoid the conflict between the definition of the multivariate Fox's H-function and the analytical expressions.
- We derive highly accurate and simplified closed-form approximations for the studied performance metrics by using a single $\mathcal{F}$ distribution. Furthermore, we pursue an asymptotic performance analysis in the high-SNR regime. The derived results can provide useful insights into the effects of different system and fading parameters on the performance.

The remainder of the paper is organized as follows. In Section II, we introduce the statistical characterizations of the $\mathcal{F}$ distribution and the definition of multivariable Fox's H-function. Exact closed-form PDF and CDF expressions of the sum of Fisher-Snedecor $\mathcal{F}$ RVs are derived in Section III. Section IV provides a single $\mathcal{F}$ distribution to approximate the distribution of sum of $\mathcal{F}$ RVs using the moment matching method for the first, second and third moments, and the KS goodness-of-fit statistical test is evaluated. In Section V, we investigate the performance in several wireless communications scenarios, and present simple asymptotic expressions. Section VI provides the numerical results and the accuracy of the obtained expressions is validated via Monte Carlo simulations. Finally, Section VII concludes this paper.

II. PRELIMINARIES

A. STATISTICS OF FISHER-SNEDECOR $\mathcal{F}$ RANDOM VARIABLES

The PDF and CDF of the instantaneous SNR, γ, at the destination over Fisher-Snedecor $\mathcal{F}$ fading channels are, respectively, given by [29, eq. (6)], [29, eq. (12)].

$$f_\gamma(\gamma) = \frac{m^m (m_s-1)^{m_s} \bar{\gamma}^{m_s} \gamma^{m-1}}{B(m,m_s)(m\gamma + (m_s-1)\bar{\gamma})^{m+m_s}}, \tag{1}$$

and

$$F_\gamma(\gamma) = \frac{m^{m-1}\gamma^m}{B(m,m_s)(m_s-1)^m \bar{\gamma}^m} \times {}_2F_1\left(m, m+m_s, m+1; -\frac{m\gamma}{(m_s-1)\bar{\gamma}}\right), \tag{2}$$

where $B(\cdot,\cdot)$ denotes the beta function [30, eq. (8.38)]; ${}_2F_1(\cdot)$ denotes the Gauss hypergeometric function [30, eq. (9.10)] and $m_s > 1$; the parameters m, m_s, and $\overline{\gamma}$ denote the number of multipath clusters, shadowing shape, and average SNR, respectively

The MGF of γ is given by [29, eq. (10)]

$$\mathcal{M}_\gamma(s) = {}_1F_1\left(m; 1-m_s; \frac{s\bar{\gamma}(m_s-1)}{m}\right) + \frac{\Gamma(-m_s)\left(\frac{s\bar{\gamma}(m_s-1)}{m}\right)^{m_s}}{B(m,m_s)} \times {}_1F_1\left(m+m_s; 1+m_s; \frac{s\bar{\gamma}(m_s-1)}{m}\right), \quad (3)$$

where ${}_1F_1(\cdot,\cdot,\cdot)$ denotes the Kummer confluent hypergeometric function [30, eq. (9.210.1)]. Using the definition of Tricomi confluent hypergeometric function [30, eq. (9.210.2)], after some algebraic manipulations, we obtain

$$\mathcal{M}_\gamma(s) = \frac{\Gamma(m+m_s)}{\Gamma(m_s)}\Psi\left(m, 1-m_s; \frac{s\bar{\gamma}(m_s-1)}{m}\right), \quad (4)$$

where $\Psi(\cdot,\cdot;\cdot)$ is the Tricomi confluent hypergeometric function, which can be expressed as the Meijer's G-function [30, eq. (9.301)], and (4) can be written as in [23, eq. (2)].

The nth moment of the Fisher-Snedecor $\mathcal{F}$ distribution can be derived in closed-form as [29, eq. (9)]. With the aid of [30, eq. (8.384.1)], one obtains

$$\mathrm{E}\left[\gamma^n\right] = \left(\frac{(m_s-1)\bar{\gamma}}{m}\right)^n \frac{B(m+n, m_s-n)}{B(m,m_s)}, \quad (5)$$

where $\mathrm{E}[\,\cdot\,]$ denotes the mathematical expectation.

B. MULTIVARIABLE FOX'S H-FUNCTION

Multivariable Fox's H-function has several notations. Among them, we choose a widely adopted notation given as [31, eq. (A.1)] which is shown as (6) at the bottom of the page, where $j \triangleq \sqrt{-1}$,

$$\Psi(\zeta_1,\ldots,\zeta_r) = \frac{\prod_{j=1}^{n}\Gamma\left(1-a_j+\sum_{i=1}^{r}\alpha_j^{(i)}\zeta_i\right)}{\prod_{j=n+1}^{p}\Gamma\left(a_j-\sum_{i=1}^{r}\alpha_j^{(i)}\zeta_i\right)} \times \left(\prod_{j=1}^{q}\Gamma\left(1-b_j+\sum_{i=1}^{r}\beta_j^{(i)}\zeta_i\right)\right)^{-1}, \quad (7)$$

and

$$\phi_i(\zeta_i) = \frac{\prod_{\lambda=1}^{m_i}\Gamma\left(d_\lambda^{(i)}-\delta_\lambda^{(i)}\zeta_i\right)\prod_{j=1}^{n_i}\Gamma\left(1-c_j^{(i)}+\gamma_j^{(i)}\zeta_i\right)}{\prod_{j=n_i+1}^{p_i}\Gamma\left(c_j^{(i)}-\gamma_j^{(i)}\zeta_i\right)\prod_{\lambda=m_i+1}^{q_i}\Gamma\left(1-d_\lambda^{(i)}+\delta_\lambda^{(i)}\zeta_i\right)}. \quad (8)$$

Although the numerical evaluation for multivariate Fox's H-function is unavailable in popular mathematical packages such as MATLAB and Mathematica, many implementations have been reported [25]–[28]. For example, two Mathematica implementations of the single Fox's H-function are provided in [25] and [27] using the Mellin Barnes integral. Although both the Lauricella multivariate hypergeometric function and the multivariate Fox's H-function can be calculated using multiple contour integral of Mellin-Barnes type, the calculation of L-fold Mellin-Barnes integral is inefficient because the integration will be more difficult to converge as L increases. Thus, the calculation time will be large. Furthermore, for the multivariate Fox's H-function, an efficient GPU-oriented MATLAB routine was introduced in [26, Appendix C]. By translating the Mellin-Barnes contour constraints into a linear optimization problem, a code automating the contour definition was also proposed in [26, Appendix D]. Moreover, a Python implementation for the multivariable Fox's H-function was presented in [28] by estimating a multivariate integral using simple rectangle quadrature. In the following, we utilize the efficient Python implementation to evaluate our results. The code can provide accurate results, i.e., its execution time for ternary Fox's H-function is less than a few seconds. If we use the Mellin Barnes integral, it takes much longer time (e.g., more than ten minutes) to obtain the same result.

III. SUM OF FISHER-SNEDECOR $\mathcal{F}$ RANDOM VARIABLES

In this section, we investigate the statistical characterization of the sum of Fisher-Snedecor $\mathcal{F}$ RVs and derive exact closed-form expressions for PDF and CDF. Let $z \triangleq$

$$H[z_1,\ldots,z_r] \triangleq H_{p,q:p_1,q_1;\ldots;p_r,q_r}^{0,n:m_1,n_1;\ldots;m_r,n_r}\left[\begin{array}{c|l} z_1 & \left(a_j;\alpha_j^{(1)},\ldots,\alpha_j^{(r)}\right)_{1,p} : \left(c_j^{(1)},\gamma_j^{(1)}\right)_{1,p_1};\cdots;\left(c_j^{(r)},\gamma_j^{(r)}\right)_{1,p_r} \\ \vdots & \\ z_r & \left(b_j;\beta_j^{(1)},\ldots,\beta_j^{(r)}\right)_{1,q} : \left(d_j^{(1)},\delta_j^{(1)}\right)_{1,q_1};\cdots;\left(d_j^{(r)},\delta_j^{(r)}\right)_{1,q_r} \end{array}\right] = \frac{1}{(2\pi j)^r}\int_{L_1}\cdots\int_{L_r}\Psi(\zeta_1,\ldots,\zeta_r)\left\{\prod_{i=1}^{r}\phi_i(\zeta_i)z_i^{\zeta_i}\right\}d\zeta_1\cdots d\zeta_r \quad (6)$$

$\gamma_1+\gamma_2+\cdots+\gamma_L$, where $\gamma_\ell \sim \mathcal{F}(\overline{\gamma}_\ell, m_\ell, m_{s_\ell})$ $(\ell = 1, \ldots, L)$ are i.n.i.d. Fisher-Snedecor $\mathcal{F}$ RVs.

Theorem 1: The PDF of the sum of Fisher-Snedecor $\mathcal{F}$ RVs z is given by

$$f_Z(z) = \frac{1}{z\prod_{\ell=1}^{L}\Gamma(m_\ell)\Gamma\left(m_{s_\ell}\right)} H_{\text{PDF}}, \tag{9}$$

where

$$H_{\text{PDF}} \triangleq H_{L-1,0:2,1;0,0;\cdots;0,0;0,1}^{0,L-1:1,2;0,0;\cdots;0,0;0,0} \times \left(\begin{matrix} A_1/A_2 \\ \vdots \\ A_{L-1}/A_L \\ zA_L \end{matrix} \middle| \begin{matrix} v_2, \ldots, v_L : (1,1), \left(1-m_{s_1}, 1\right); - \\ -:(m_1,1);(1,1) \end{matrix} \right), \tag{10}$$

and

$$\begin{cases} A_\ell \triangleq m_\ell/\left(\bar{\gamma}_\ell\left(m_{s_\ell}-1\right)\right) \ (\ell = 1, \ldots, L), \\ A_{L+1} = 1, \\ \mu_k = \underbrace{0, \ldots, 0}_{k-2}, 1, -1, \underbrace{0, \ldots, 0}_{L}, \\ \bar{\mu}_k = \underbrace{0, \ldots, 0}_{k-2}, -1, 1, \underbrace{0, \ldots, 0}_{L}, \\ v_k = (1-m_k; \mu_k), (1; \bar{\mu}_k), \left(1-m_{s_k}; \bar{\mu}_k\right). \end{cases} \tag{11}$$

Proof: Please refer to Appendix A. ■

Theorem 2: The CDF of the sum of Fisher-Snedecor $\mathcal{F}$ RVs z is given by

$$F_Z(z) = \frac{1}{\prod_{\ell=1}^{L}\Gamma(m_\ell)\Gamma\left(m_{s_\ell}\right)} H_{\text{CDF}}, \tag{12}$$

where

$$H_{\text{CDF}} \triangleq H_{L-1,0:2,1;0,0;\cdots;0,0;0,1}^{0,L-1:1,2;0,0;\cdots;0,0;0,0} \times \left(\begin{matrix} A_1/A_2 \\ \vdots \\ A_{L-1}/A_L \\ zA_L \end{matrix} \middle| \begin{matrix} v_2, \ldots, v_L : (1,1), \left(1-m_{s_1}, 1\right); - \\ -:(m_1,1);(0,1) \end{matrix} \right). \tag{13}$$

Proof: Following similar procedures as in Appendix A, we can derive the CDF of z by taking the inverse Laplace transform of $M_z(s)/s$. ■

For the i.i.d. case, we have $A_\ell/A_{\ell+1} = 1$. Thus, eqs. (9) and (12) can be calculated more efficiently.

IV. ACCURATE CLOSED-FORM APPROXIMATIONS

In this section, we present accurate closed-form approximations to the distribution of a sum of Fisher-Snedecor $\mathcal{F}$ RVs using a single Fisher-Snedecor $\mathcal{F}$ RV,[1] which can be used to provide more insights into the impact of the parameters on the overall system performance. The parameters $\bar{\gamma}$, $m_{\mathcal{F}}$ and $m_{s_{\mathcal{F}}}$ are obtained using the moment matching method for the first, second and third moments.

A. SINGLE $\mathcal{F}$ APPROXIMATION TO THE SUM OF SQUARED $\mathcal{F}$-DISTRIBUTED RVS

Theorem 3: For the sum of i.n.i.d. $\mathcal{F}$ RVs, the parameters of single $\mathcal{F}$ distribution are given by

$$\begin{cases} \bar{\gamma}_{\mathcal{F}} = \sum_{i=1}^{L}\bar{\gamma}_i, \\ m_{\mathcal{F}} = -\frac{2(H_{\mathcal{F}}-Y_{\mathcal{F}})}{H_{\mathcal{F}}-2Y_{\mathcal{F}}+H_{\mathcal{F}}Y_{\mathcal{F}}}, \\ m_{s_{\mathcal{F}}} = \frac{4H_{\mathcal{F}}-3Y_{\mathcal{F}}-1}{2H_{\mathcal{F}}-Y_{\mathcal{F}}-1}, \end{cases} \tag{14}$$

where $H_{\mathcal{F}}$ and $Y_{\mathcal{F}}$ can be calculated as

$$\begin{aligned} H_{\mathcal{F}} &\triangleq \frac{\sum_{\ell=1}^{L}(H_\ell-\varepsilon_\ell-1)\bar{\gamma}_\ell^2}{\left(\sum_{\ell=1}^{L}\bar{\gamma}_\ell\right)^2}+1, \\ Y_F &\triangleq \frac{\sum_{\ell=1}^{L}(H_\ell Y_\ell-\varepsilon_\ell Y_\ell-1)\bar{\gamma}_\ell^3+\left(\sum_{\ell=1}^{L}\bar{\gamma}_\ell\right)^3-3\sum_{\ell=1}^{L}(H_\ell-\varepsilon_\ell-1)\bar{\gamma}_\ell^3}{\left(\sum_{\ell=1}^{L}\bar{\gamma}_\ell\right)\left(\sum_{\ell=1}^{L}(H_\ell-\varepsilon_\ell-1)\bar{\gamma}_\ell^2+\left(\sum_{\ell=1}^{L}\bar{\gamma}_\ell\right)^2\right)} \\ &\quad + \frac{3\left(\sum_{\ell=1}^{L}(H_\ell-\varepsilon_\ell-1)\bar{\gamma}_\ell^2\right)}{\left(\sum_{\ell=1}^{L}(H_\ell-\varepsilon_\ell-1)\bar{\gamma}_\ell^2+\left(\sum_{\ell=1}^{L}\bar{\gamma}_\ell\right)^2\right)}, \end{aligned} \tag{15}$$

where $H_\ell = \frac{(1+m_\ell)(m_{s_\ell}-1)}{m_\ell(m_{s_\ell}-2)}$ $(\ell = 1, \ldots, L)$, $Y_\ell = \frac{(m_{s_\ell}-1)(2+m_\ell)}{m_\ell(m_{s_\ell}-3)}$ and ε_ℓ is the factor that can be adjusted to minimize the difference between the approximate and the exact statistics. For example, we can choose ε_ℓ to minimize the Kolmogorov distance.[2]

For the i.i.d case, let $H_\ell = H$ $(\ell = 1, \ldots, L)$, $Y_\ell = Y$, $m = m_\ell$, $m_s = m_{s_\ell}$, $\varepsilon = \varepsilon_\ell$, $\bar{\gamma} = \bar{\gamma}_\ell$, so the parameters of single $\mathcal{F}$ distribution are given by

$$\begin{cases} \bar{\gamma}_{\mathcal{F}} = L\bar{\gamma}, \\ m_{\mathcal{F}} = -\frac{2(H_{\mathcal{F}}-Y_{\mathcal{F}})}{H_{\mathcal{F}}-2Y_{\mathcal{F}}+H_{\mathcal{F}}Y_{\mathcal{F}}}, \\ m_{s_{\mathcal{F}}} = \frac{4H_{\mathcal{F}}-3Y_{\mathcal{F}}-1}{2H_{\mathcal{F}}-Y_{\mathcal{F}}-1}, \end{cases} \tag{16}$$

where

$$\begin{cases} H_{\mathcal{F}} \triangleq \frac{(H-\varepsilon-1)}{L}+1, \\ Y_{\mathcal{F}} \triangleq \frac{(H-\varepsilon)Y+L^2+3L(H-\varepsilon)-3L-3(H-\varepsilon)+2}{L(H-\varepsilon)-L+L^2}. \end{cases} \tag{17}$$

Proof: Please refer to Appendix B. ■

1. With the help of (A-2) and (A-5), we can re-write the MGF of a sum of Fisher-Snedecor $\mathcal{F}$ RVs and the MGF of a single Fisher-Snedecor $\mathcal{F}$ RV as Mellin-Barnes integrals, and observe that they are similar to each other. In addition, using the MATLAB distribution fit tool, it also has been observed that the single Fisher-Snedecor $\mathcal{F}$ distribution can serve as an efficient approximation to the sum of Fisher-Snedecor $\mathcal{F}$ distribution.

2. Note that obtaining the exact closed-form expression for the optimal value of ε_ℓ is difficult, if not impossible. However, the CDF can be calculated efficiently by using the Python code. Thus, using the fading parameters involved in the sum of RVs, we can perform the KS goodness-of-fit test easily to obtain the ε_{opt} by minimizing the largest absolute difference between the analytical and empirical CDFs. Thus, the optimal values of the adjustment factor for different small-scale and shadowing parameters are given in Fig. 2. By using ε_{opt}, we prove that the approximate results can match the exact ones and Monte Carlo simulations well in Section VI.

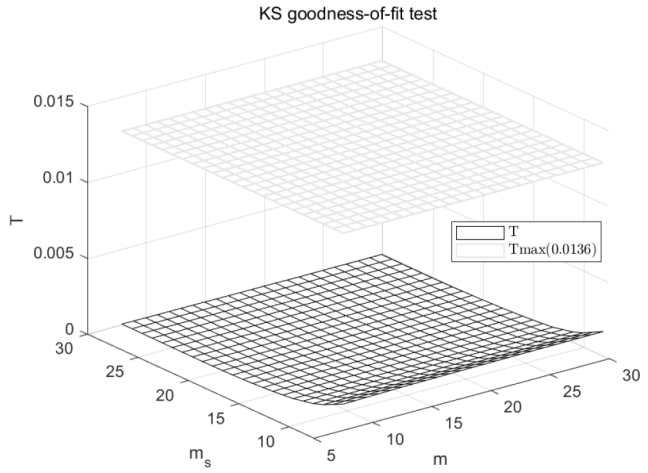

FIGURE 1. KS goodness-of-fit test statistic for the exact and the approximate distributions with 5% significance level for $L = 2$.

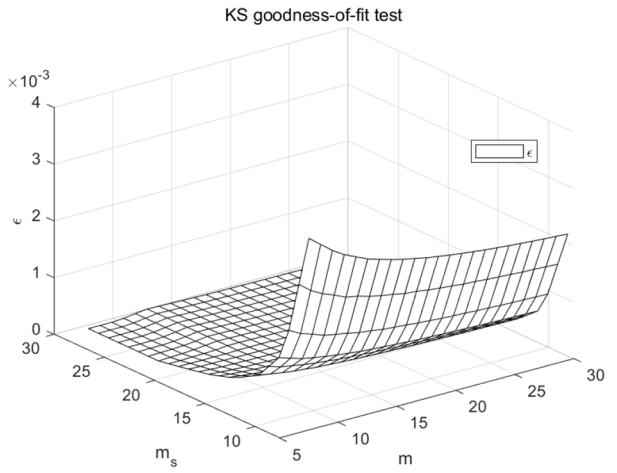

FIGURE 2. Adjustment factor that minimizes the absolute value of the difference between the exact and the approximate distributions for $L = 2$.

B. KS GOODNESS-OF-FIT TEST

KS goodness-of-fit statistical test can be used to test the accuracy of the proposed approximations [32], [33]. The KS test is defined as the largest absolute difference between two CDFs, which can be expressed as

$$T \triangleq \max\left|F_Z(z) - F_{\hat{Z}}(z)\right|, \tag{18}$$

where $F_Z(z)$ is the analytical CDF of RV Z and $F_{\hat{Z}}(z)$ is the empirical CDF of RV $\hat{Z}$.

Let us define H_0 as the null hypothesis under which the observed data of $\hat{Z}$ belong to the CDF of the approximate distribution $F_Z(z)$. Hypothesis H_0 is accepted if $T < T_{\max}$. The critical value $T_{\max} = \sqrt{-(1/2v)\ln(\alpha/2)}$ corresponds to a significance level of α [32].

Without loss of generality, we consider a sum of two i.i.d. Fisher-Snedecor $\mathcal{F}$ RVs with channel parameters $m = m_\ell$ and $m_s = m_{s_\ell}$ $(\ell = 1, 2)$. The average SNR is set by $\bar{\gamma} = \bar{\gamma}_\ell = 1$ dB. The exact results of CDF have been obtained by averaging at least $v = 10^4$, and one obtains $T_{\max} = 0.0136$ for $\alpha = 5\%$. Fig. 1 depicts the KS test statistic for different combinations of m and m_s, and the corresponding optimal adjustment factor ε is shown in the Fig. 2. It is obvious that H_0 is accepted with 95% significance for different settings of parameters. In conclusion, the single $\mathcal{F}$ distribution is a highly accurate approximation to the sum of $\mathcal{F}$ RVs.

V. APPLICATIONS TO WIRELESS COMMUNICATIONS

In this section, we present six applications in wireless communication systems, including OP, effective capacity, and channel capacities under four different adaptive transmission strategies. We assume communication over a fading channel that follows Fisher-Snedecor $\mathcal{F}$ distribution and a diversity receiver employs MRC.

A. OUTAGE PROBABILITY

The OP is defined as the probability that the instantaneous SNR is less than a predetermined threshold γ_{th}. The combiner output SNR Z is simply the sum of the individual branches SNRs and the OP can be directly calculated as

$$P_{\text{out}} = P(Z < \gamma_{\text{th}}) = F_Z(\gamma_{\text{th}}), \tag{19}$$

where γ_{th} is the minimum usable SNR threshold. Therefore, the OP of the MRC receiver can be directly evaluated by using (12).

Proposition 1: A highly accurate and simple approximation of OP can be derived using single $\mathcal{F}$ fading channel as

$$P_{\text{o},\mathcal{F}} \simeq \frac{{m_\mathcal{F}}^{m_\mathcal{F}-1}{\gamma_{\text{th}}}^{m_\mathcal{F}}}{B\left(m_\mathcal{F}, m_{s_\mathcal{F}}\right)\left(m_{s_\mathcal{F}} - 1\right)^{m_\mathcal{F}}\bar{\gamma}_\mathcal{F}^{m_\mathcal{F}}} \times {}_2F_1\left(m_\mathcal{F}, m_\mathcal{F} + m_{s_\mathcal{F}}, m_\mathcal{F} + 1; -\frac{m_\mathcal{F}\gamma_{\text{th}}}{\left(m_{s_\mathcal{F}} - 1\right)\bar{\gamma}_\mathcal{F}}\right). \tag{20}$$

The asymptotic expansions of the OP for high SNRs can be obtained by computing the residue [28]. Let us consider the residue at the points $\zeta = (\zeta_1, \ldots, \zeta_L)$, where $\zeta_\ell = \min_{j=1,\ldots,m_\ell}(d_j^{(\ell)}/\delta_j^{(\ell)})$ $(\ell = 1, \ldots, L)$. We obtain the approximate OP expression as

$$P_{\text{o,appr}} \simeq \frac{1}{\Gamma\left(1 + \sum_{\ell=1}^{L} m_\ell\right)} \prod_{\ell=1}^{L} \frac{\Gamma\left(m_{s_\ell} + m_\ell\right)}{\Gamma\left(m_{s_\ell}\right)} \left(\frac{\gamma_{\text{th}} m_\ell}{\bar{\gamma}_\ell\left(m_{s_\ell} - 1\right)}\right)^{m_\ell}. \tag{21}$$

B. EFFECTIVE CAPACITY

With the developments of modern wireless communication, a wide range of services with diverse Quality of Service (QoS) requirements have sprung up, leading to a growing need for QoS guarantees such as different bandwidth and delay constraints. However, because the wireless channel suffers from time-varying fading impairments, the channel capacity based on the concept of Shannon capacity is insufficient to characterize the effective transmission data rate. The effective capacity, which accounts for the achievable

capacity subject to the incurred latency relating to the corresponding buffer occupancy, is a useful and insightful information theoretic measure particularly in emerging technologies [13], [34]–[38]. The effective capacity normalized by the bandwidth can be defined as [39, eq. (11)]

$$C_{\text{eff}} = -\frac{1}{A}\log_2\left(\int_0^\infty \frac{1}{(1+z)^A} f_z(z)dz\right) \quad \text{bit /s/Hz}, \tag{22}$$

where $z = \sum_{\ell=1}^{L} \gamma_\ell$, $\gamma_\ell \sim \mathcal{F}(\overline{\gamma}_\ell, m_\ell, m_{s_\ell})$ $(\ell = 1, \ldots, L)$, and

$$A = \frac{BT\theta}{\ln 2} \tag{23}$$

is a delay constraint with the asymptotic decay rate of the buffer occupancy θ, system bandwidth B and the block length T.

Proposition 2: For the i.n.i.d. case, the effective capacity can be deduced as

$$C_{\text{eff}} = -\frac{1}{A}\log_2\left(\frac{A}{\Gamma(1+A)}\prod_{\ell=1}^{L}\frac{1}{\Gamma(m_\ell)\Gamma\left(m_{s_\ell}\right)} H_{\text{eff}}\right), \tag{24}$$

where

$$H_{\text{eff}} \triangleq H_{L-1,0:2,1;0,0;\cdots;0,0;1,2}^{0,L-1:1,2;0,0;\cdots;0,0;1,1} \times \left(\begin{matrix} A_1/A_2 \\ \vdots \\ A_{L-1}/A_L \\ A_L \end{matrix}\middle| \begin{matrix} \nu_2, \ldots, \nu_L : (1,1), \left(1-m_{s_1}, 1\right); (1,1) \\ -:(m_1,1); (A,1), (0,1) \end{matrix}\right). \tag{25}$$

Proof: Please refer to Appendix C. ■

Remark 1: A highly accurate approximation of effective capacity can be derived using a single $\mathcal{F}$ fading channel by setting $L = 1$ in (24). After some algebraic manipulations, we obtain the same result as [29, eq. (33)] which provides useful insights because it can be used as a benchmark for the derivation of simpler approximations or bounds. The approximation of effective capacity in the high-SNR region under $\mathcal{F}$ fading channels was also derived as [29, eq. (41)], which can be used as the approximation of (24).

C. CHANNEL CAPACITY

In the following, we analyze the channel capacity performance under four different adaptive transmission schemes, namely CIFR, TIFR, ORA and OPRA.

1) CHANNEL INVERSION WITH FIXED RATE

CIFR ensures a fixed data rate at the receiver by inverting the channel and adapting the transmit power. The channel capacity under CIFR is defined as [40]

$$C_{\text{CIFR}} = B\log_2\left(1 + \frac{1}{\int_0^\infty \frac{f_Z(z)}{z}dz}\right). \tag{26}$$

Proposition 3: The channel capacity under CIFR can be expressed as

$$C_{\text{CIFR}} = B\log_2\left(1 + \frac{1}{\prod_{\ell=1}^{L}\frac{s}{\Gamma(m_{s_\ell})\Gamma(m_\ell)} H_{\text{CIFR}}}\right), \tag{27}$$

where

$$H_{\text{CIFR}} \triangleq H_{L-1,0:2,1;0,0;\cdots;0,0;1,1}^{0,L-1:1,2;0,0;\cdots;0,0;0,1} \times \left(\begin{matrix} A_1/sA_2 \\ \vdots \\ A_{L-1}/sA_L \\ A_L/s \end{matrix}\middle| \begin{matrix} \nu_2, \ldots, \nu_L : (1,1), \left(1-m_{s_1}, 1\right); (2,1) \\ -:(m_1,1); (1,1) \end{matrix}\right) \tag{28}$$

and s is a number close to zero (e.g., $s = 10^{-6}$).

Proof: Please refer to Appendix D. ■

Remark 2: With the aid of Theorem 3, a highly accurate approximation of the channel capacity per unit bandwidth under CIFR can be deduced using single $\mathcal{F}$ fading channel. Setting $L = 1$ in (27) and we obtain the same result as [9, eq. (23)] after some algebraic manipulations. Notice that [9, eq. (23)] is insightful and we can observe that m and m_s have the same influence to the channel capacity under CIFR approximately. Besides, it is easy to see that the channel capacity under CIFR increases as m and m_s increase. Under the $\mathcal{F}$ composite fading channel, a high SNR approximation of channel capacity under CIFR was derived as [9, eq. (26)], which can be used as the high-SNR approximation of (27).

2) TRUNCATED CHANNEL INVERSION WITH FIXED RATE

Another approach is to use a modified inversion policy that inverts the channel fading only above a fixed cutoff fade depth. The channel capacity under TIFR policy is defined as

$$C_{\text{TIFR}} = B\log_2\left(1 + \frac{1}{\int_{z_0}^\infty \frac{f_Z(z)}{z}dz}\right)\int_{z_0}^\infty f_Z(z)dz, \tag{29}$$

where z_0 is a cutoff level that can be selected to achieve a specified outage probability or to maximize (29). Notice that (29) reduces to (26) when z_0 approaches zero.

Proposition 4: The closed-form expression for the capacity under TIFR is given by

$$C_{\text{TIFR}} = B\log_2\left(1 + \frac{1}{\frac{1}{z_0}\prod_{\ell=1}^{L}\frac{1}{\Gamma(m_{s_\ell})\Gamma(m_\ell)} H_{\text{TIFR}}}\right) \times \left(1 - \prod_{\ell=1}^{L}\frac{1}{\Gamma\left(m_{s_\ell}\right)\Gamma(m_\ell)} H_{\text{CDF}}\right), \tag{30}$$

where

$$H_{\mathrm{TIFR}} \triangleq H_{L-1,0:2,1;0,0;\cdots;0,0;1,2}^{0,L-1:1,2;0,0;\cdots;0,0;1,0} \times \left(\begin{matrix} z_0A_1/A_2 \\ \vdots \\ z_0A_{L-1}/A_L \\ z_0A_L \end{matrix} \middle| \begin{matrix} \nu_2, \ldots, \nu_L : (1,1), \left(1-m_{s_1},1\right); (2,1) \\ -:(m_1,1);\ (1,1)(1,1) \end{matrix} \right). \tag{31}$$

Proof: Please refer to Appendix E. ■

Remark 3: Using Theorem 3, an accurate approximation of the channel capacity under TIFR can be derived by single $\mathcal{F}$ fading channel. Substituting $L = 1$ in (30), after some algebraic manipulations, we can get the same result as [9, eq. (27)] and [9, eq. (28)]. An approximation of channel capacity under TIFR in the high-SNR region is given by [9, eq. (30)], which can be used as the high SNR approximation of (30) with the aid of (14).

3) OPTIMAL RATE ADAPTATION WITH CONSTANT TRANSMIT POWER

The channel capacity under ORA with a constant transmit power is given by [40, eq. (29)]

$$C_{\mathrm{ORA}} = B \int_0^{\infty} \log_2(1+z) f_Z(z) dz. \tag{32}$$

Proposition 5: Under the ORA scheme, the channel capacity can be expressed as

$$C_{\mathrm{ORA}} = \frac{B}{s \ln(2)} \prod_{\ell=1}^{L} \frac{1}{\Gamma\left(m_{s_\ell}\right)\Gamma(m_\ell)} H_{ORA}, \tag{33}$$

where

$$H_{\mathrm{ORA}} \triangleq H_{L+3,0:2,1;0,0;\cdots;0,0;0,1;1,2}^{0,L+2:1,2;0,0;\cdots;0,0;0,0;1,1} \times \left(\Delta_{\mathrm{ORA}} \middle| \begin{matrix} \nu'_2, \cdots, \nu'_L, (0;0,\cdots,0,-1,-1), (0;0,\cdots,0,-1,-1), \\ -:(m_1,1);\ (1,1);\ (1,1),(0,1) \\ (1;0,\cdots,0,1,1), (2;0,\cdots,0,1,1) : (1,1), \left(1-m_{s_1},1\right);\ -;\ (1,1) \\ - \end{matrix} \right), \tag{34}$$

$\nu'_k = (1-m_k;\mu_k,0), (1;\bar{\mu}_k,0), (1-m_{s_k};\bar{\mu}_k,0)$ and $\Delta_{\mathrm{ORA}} \triangleq (A_1/A_2, \ldots, A_{L-1}/A_L, A_L, s)^{\mathrm{T}}$.

Proof: Please refer to Appendix F. ■

Remark 4: With the help of Theorem 3, channel capacity under ORA has a tight approximation which can be derived using single $\mathcal{F}$ fading channel. Substituting (D-2) into (D-1) and letting $L = 1$, we obtain the same result as [9, eq. (19)]. An approximation of [9, eq. (19)] in the high-SNR region is given by [29, eq. (26)]. Using (14), we obtain a simple algebraic representation of the approximation of channel capacity under ORA in the high-SNR region as [29, eq. (26)], which also provides useful insights on the impact of the involved parameters. For example, it is evident that eq. (26) in [29] can be expressed in terms of $\overline{\gamma_{\mathcal{F}}}$. This transformation is useful in quantifying the average SNR value under different fading conditions.

4) OPTIMAL POWER AND RATE ADAPTATION

Under OPRA, the channel capacity is given by [41, eq. (7)]

$$C_{\mathrm{OPRA}} = B \int_{\gamma_0}^{\infty} \log_2\left(\frac{z}{\gamma_0}\right) f_Z(z) dz, \tag{35}$$

where γ_0 is the cutoff carrier-to-noise ratio value. No data is sent below γ_0, and γ_0 must satisfy [41, eq. (6)]

$$\int_{\gamma_0}^{\infty} \left(\frac{1}{\gamma_0} - \frac{1}{z}\right) f_Z(z) dz = 1. \tag{36}$$

Let

$$S(z) = \begin{cases} \frac{1}{\gamma_0} - \frac{1}{z} & z \geq \gamma_0, \\ 0 & \text{otherwise}, \end{cases} \tag{37}$$

the channel capacity under OPRA can also be written as

$$C_{\mathrm{OPRA}} = B \int_0^{\infty} \log_2(1 + S(z)z) f_Z(z) dz. \tag{38}$$

Proposition 6: The channel capacity under OPRA is derived as

$$C_{\mathrm{OPRA}} = \prod_{\ell=1}^{L} \frac{1}{\Gamma(m_\ell)\Gamma\left(m_{s_\ell}\right)} H_{\mathrm{OPRA}}, \tag{39}$$

where

$$H_{\mathrm{OPRA}} \triangleq H_{L+3,0:2,1;0,0;\cdots;0,0;0,1;1,1}^{0,L+1:1,2;0,0;\cdots;0,0;0,1;0,1} \times \left(\Delta_{\mathrm{OPRA}} \middle| \begin{matrix} \nu'_2, \cdots, \nu'_L, (1;0,\ldots,0,-1,-1), (1;0,\cdots,0,-1,-1), \\ -:(m_1,1);\ (1,1);\ (0,1) \\ (1;0,\ldots,0,1,1), (1;0,\ldots,0,1,1) : (1,1), \left(1-m_{s_1},1\right);\ -;\ - \\ - \end{matrix} \right) \tag{40}$$

and $\Delta_{\mathrm{OPRA}} \triangleq (\gamma_0 A_1/A_2, \ldots, \gamma_0 A_{L-1}/A_L, \gamma_0 A_L, s)^{\mathrm{T}}$.

Proof: Please refer to Appendix G. ■

Remark 5: Based on Theorem 3, a tight approximation of channel capacity under OPRA can be derived using single $\mathcal{F}$ fading channel. Substituting (D-3) into (D-1) and letting $L = 1$, the same result as [29, eq. (52)] is obtained. Note that [29, eq. (52)] is suitable for analysis both analytically and numerically and can used as a benchmark for further derivation of an approximation. In the high-SNR regime, the approximation of (39) is given as [29, eq. (57)].

Remark 6: To determine the value of γ_0, we can rewrite (36) as

$$\frac{1}{\gamma_0} \underbrace{\int_{\gamma_0}^{\infty} f_Z(z) dz}_{I_8} - \underbrace{\int_{\gamma_0}^{\infty} \frac{f_Z(z)}{z} dz}_{I_9} = 0, \tag{41}$$

where I_8 and I_9 have been solved in (D-1) and (D-4) respectively. Thus, it follows that

$$0 = \frac{1}{\gamma_0} \left(1 - \prod_{\ell=1}^{L} \frac{1}{\Gamma\left(m_{s_\ell}\right)\Gamma(m_\ell)} H_{\mathrm{CDF}} \right) - \prod_{\ell=1}^{L} \frac{1}{\Gamma\left(m_{s_\ell}\right)\Gamma(m_\ell)} H_{\mathrm{TIFR}}. \tag{42}$$

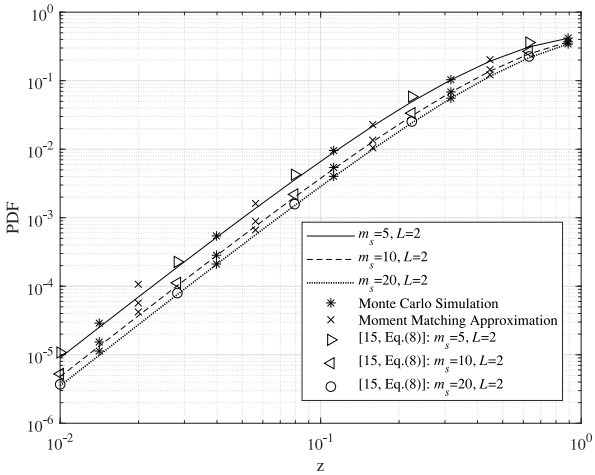

FIGURE 3. PDF for the sum of squared $\mathcal{F}$-distributed RVs.

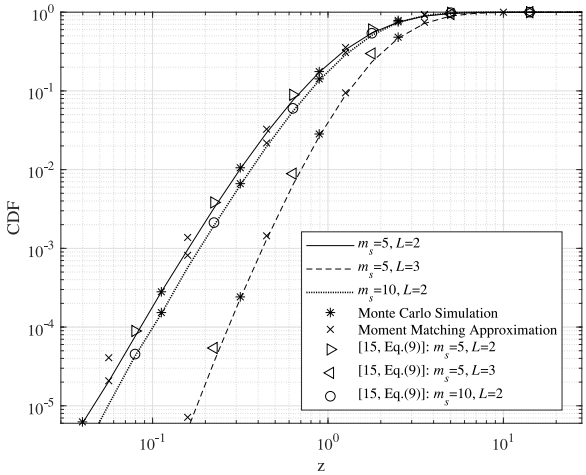

FIGURE 4. CDF for the sum of squared $\mathcal{F}$-distributed RVs.

A detailed proof of the existence of γ_0 in the range $[0, 1]$ is given in [42]. Thus, with the aid of (42), γ_0 can be solved with mathematical software and we find that using the dichotomy for iterations within 20 times can make the error less than 10^{-6}.

Remark 7: Channel capacity in AWGN, in bits per second, is given by Shannons formula as [43]

$$C_{\text{AWGN}} = B\log_2(1+z). \tag{43}$$

The relationship of C_{ORA}, C_{OPRA} and C_{AWGN} can be obtained by applying the Jensen's inequality as [44]

$$0 \le C_{\text{OPRA}} - C_{\text{ORA}} \le \min\big(C_{\text{OPRA}}, -\log_2\gamma_0\big), \tag{44a}$$

$$C_{\text{ORA}} \le C_{\text{AWGN}} \tag{44b}$$

and there is no general order relation between C_{OPRA} and C_{AWGN}.

VI. NUMERICAL RESULTS

In this section, analytical results are presented to illustrate the proposed applications of the sum of Fisher-Snedecor $\mathcal{F}$ RVs in wireless communication systems. All results are substantiated by Monte Carlo simulations.

Figures 3 and 4, respectively, plot the PDF and CDF of the sum of Fisher-Snedecor $\mathcal{F}$ RVs and their proposed approximation obtained by moment matching method for different values of m_s and L, assuming $m_{s_\ell} = m_s$ $(\ell = 1, 2, 3)$, $m_\ell = 2$, $\gamma_\ell = 0$ dB. In both figures, it can be observed that the approximate PDFs and CDFs match the exact ones well for all considered cases. Furthermore, analytical results perfectly match Monte Carlo simulations, thus validating our results. In addition, analytical results of the PDF for the sum of Fisher-Snedecor $\mathcal{F}$ RVs given as [23, eq. (8)] are shown in Fig. 3. As it can be seen, the analytical results do not match well the Monte Carlo simulations at low-m_s values. Moreover, Fig. 4 shows the impact of different values of L. As L increases, analytical results of the CDF for the sum of Fisher-Snedecor $\mathcal{F}$ RVs given as [23, eq. (9)] are more inaccurate.

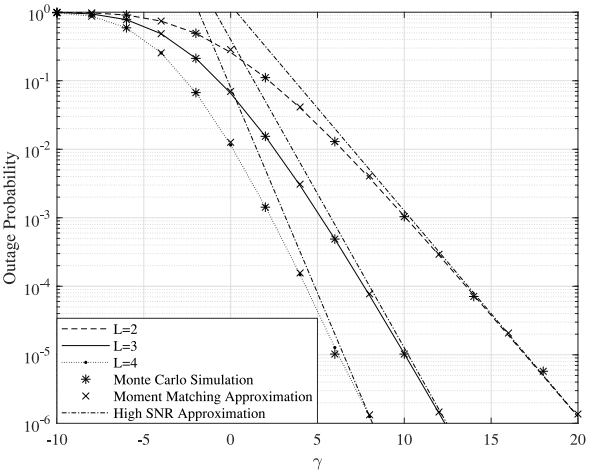

FIGURE 5. Outage probability versus average SNR for dual, triple and quadruple MRC receivers.

Figure 5 depicts the OP performance versus average SNR γ for a dual-, triple- and quadruple-branch MRC receivers with $\gamma_\ell = \gamma$ $(\ell = 1, 2, 3, 4)$, $\gamma_{\text{th}} = 0$ dB, $m_\ell = 1.5$, $m_{s_\ell} = 5$. As it can be observed, the OP decreases as the average SNR and L increase. Again, it is evident that the exact results match the approximate ones and Monte Carlo simulations well. In addition, the asymptotic expressions match well the exact ones at high SNR values thus proving their validity and versatility. The OP performance improvement is more pronounced by increasing $L = 2$ to $L = 3$.

Figures 6–9 show the analytical and simulated channel capacities versus average SNR γ under different adaptive transmission strategies respectively, assuming $L = 2$. Figs. 6 and 7 illustrate the channel capacity increases as m increases, while Figs. 8 and 9 depict the channel capacity increases as m_s increases, which means favorable system parameters can lead to a large channel capacity. Once again, perfect agreement is observed between analytical results, approximate results and Monte Carlo simulations in Figs. 6–9.

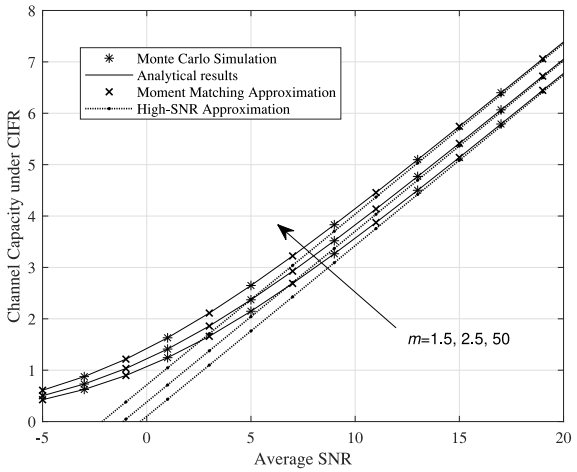

FIGURE 6. Channel capacity under CIFR versus average SNR for $L = 2$, $m_1 = m_2 = m$, $m_{s_1} = 2.5$ and $m_{s_2} = 10$.

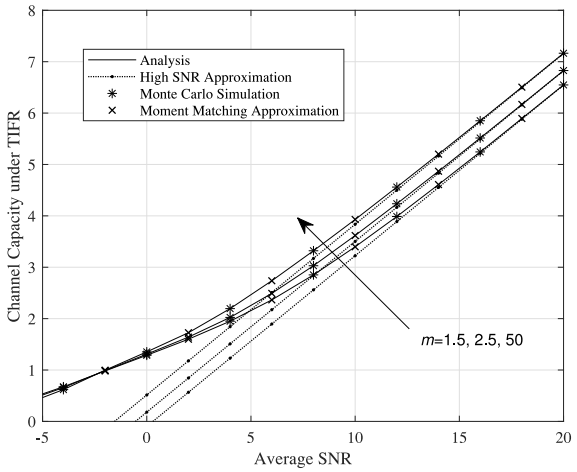

FIGURE 7. Channel capacity under TIFR versus average SNR for $L = 2$, $m_1 = m_2 = m$, $\gamma_0 = 0$ dB and $m_{s_1} = m_{s_2} = 2.5$.

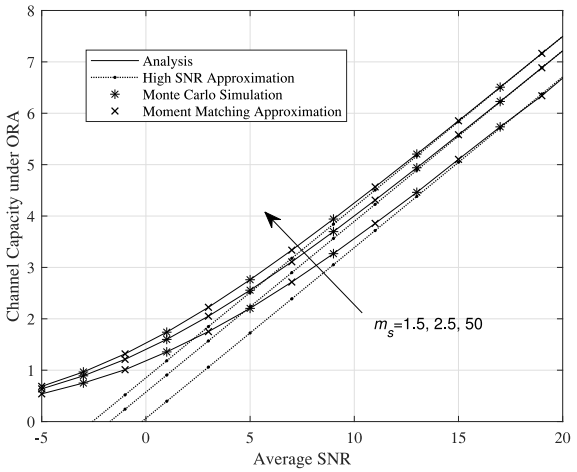

FIGURE 8. Channel capacity under ORA versus average SNR for $L = 2$, $m_{s_1} = m_{s_2} = m_s$, and $m_1 = m_2 = 2.5$.

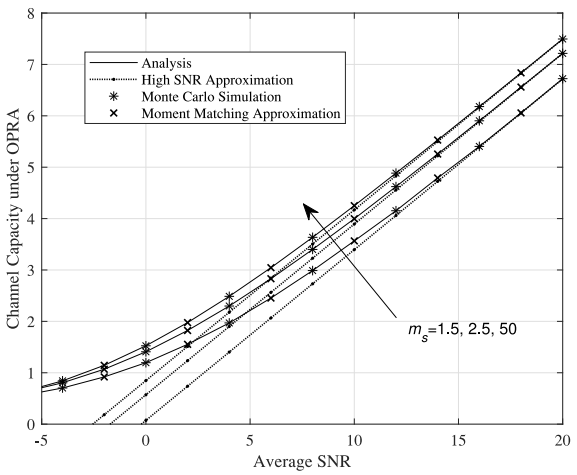

FIGURE 9. Channel capacity under OPRA versus average SNR for $L = 2$, $m_{s_1} = m_{s_2} = m_s$ and $m_1 = m_2 = 2.5$.

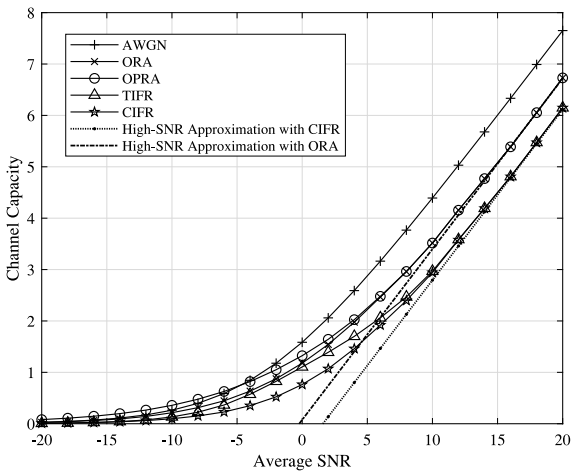

FIGURE 10. Channel capacity under four different adaptive transmission strategies versus average SNR for L=2.

As shown in Fig. 10, four different adaptive transmission strategies provide different channel capacities. Obviously, the relation we proposed in (7) is shown. As it can be observed, the channel capacity under OPRA is the largest among those adaptive transmission strategies, which is followed by the channel capacity under ORA. The channel capacity under TIFR and CIFR converges in the high-SNR regime because the asymptotic expressions of those two cases are the same for $m > 1$. This finding can be also observed in channel capacity under OPRA and ORA. Moreover, analytical and approximate results agree well with Monte Carlo simulations.

Figure 11 illustrates the effective capacity of MRC systems over i.n.i.d. $\mathcal{F}$ fading channels as a function of the delay constraint A for different settings of the parameters m_s and L, assuming $m_{s_\ell} = m_s$, $m_\ell = 5$, $\gamma_\ell = 10$ dB ($\ell = 1, 2, 3$). It can be easily observed that, the effective capacity increases as m_s and L increase. This is because of the fact that large value of m_s induces low shadowing effect and large value of L means more receive power. For a certain setting of the parameters, the effective capacity increases as A decreases (i.e., large delay). Thus, the considered system can support larger arrival rates having a larger delay constraint. Fig. 11

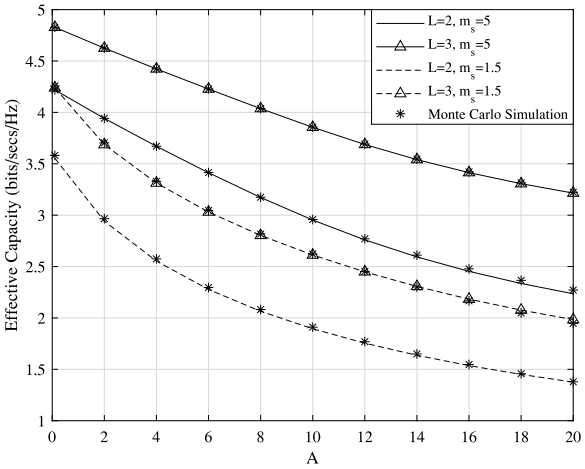

FIGURE 11. Effective capacity of MRC receivers over i.n.i.d. $\mathcal{F}$ fading channels versus the delay constraint A.

shows a perfect agreement of the Monte Carlo simulations and analytical and simulation results, which confirms the validity of the analytical result in (24).

VII. CONCLUSION

We presented exact expressions for the PDF and CDF of sum of i.n.i.d. Fisher-Snedecor $\mathcal{F}$ RVs. In addition, we proposed the single $\mathcal{F}$ distribution with an adjusted form of parameters to approximate the sum of $\mathcal{F}$ distribution by using the moment matching method. The derived results show that the introduced adjustment results closely approximate in both the lower and upper tail regions. This sufficiently accurate region-wise approximation significantly simplify the performance analysis of MRC diversity receivers over the $\mathcal{F}$ fading channels. To this end, novel, computationally efficient analytical expressions were obtained for OP, effective capacity and channel capacities under different adaptive transmission strategies. Finally, extensive numerical results have been presented to validate the proposed analytical expressions and an excellent agreement has been observed.

APPENDIX A
PROOF OF THEOREM 1

The PDF of z can be obtained as

$$f_z(z) = \mathcal{L}^{-1}\{\mathcal{M}_z(s); z\} = \frac{1}{2\pi j}\int_{\mathcal{L}} \mathcal{M}_z(s)e^{zs}ds, \quad \text{(A-1)}$$

where $\mathcal{L}^{-1}\{\cdot\}$ denotes the inverse Laplace transform and $\mathcal{M}_z(s)$ is the MGF of z. Because the Fisher-Snedecor $\mathcal{F}$ RVs are independent, we can obtain the MGF of the z using (4) as

$$\mathcal{M}_z(s) = \prod_{\ell=1}^{L} \frac{\Gamma(m_\ell + m_{s_\ell})}{\Gamma(m_{s_\ell})}\Psi\left(m_\ell; 1-m_{s_\ell}; \frac{s\bar{\gamma}_\ell(m_{s_\ell}-1)}{m_\ell}\right). \quad \text{(A-2)}$$

Substituting (A-2) into (A-1) and using [45, eq. (8.4.46.1)], we can derive the MGF of z as

$$f_z(z) = \frac{1}{2\pi j}\int_{\mathcal{L}} \prod_{\ell=1}^{L} \frac{1}{\Gamma(m_{s_\ell})\Gamma(m_\ell)} \times G_{1,2}^{2,1}\left(\frac{s\bar{\gamma}_\ell(m_{s_\ell}-1)}{m_\ell}\middle| \begin{matrix}1-m_\ell \\ 0, m_{s_\ell}\end{matrix}\right)e^{zs}ds, \quad \text{(A-3)}$$

where the integration path of $\mathcal{L}$ goes from $\sigma - \infty j$ to $\sigma + \infty j$ and $\sigma \in \mathbb{R}$.

With the aid of [30, eq. (9.301)], the product of Meijer's G-functions can be expressed as

$$\begin{aligned} I_G &\triangleq G_{1,2}^{2,1}\left(\frac{s\bar{\gamma}_1(m_{s_1}-1)}{m_1}\middle| \begin{matrix}1-m_1 \\ 0, m_{s_1}\end{matrix}\right) \\ &\quad \times \prod_{\ell=2}^{L} G_{1,2}^{2,1}\left(\frac{s\bar{\gamma}_\ell(m_{s_\ell}-1)}{m_\ell}\middle| \begin{matrix}1-m_\ell \\ 0, m_{s_\ell}\end{matrix}\right) \\ &= \frac{1}{2\pi j}\int_{\mathcal{L}_1} \Upsilon(\zeta_1)\left(\frac{A_1}{A_2}\right)^{\zeta_1}\left(\frac{A_2}{s}\right)^{\zeta_1}d\zeta_1 \\ &\quad \times \prod_{\ell=2}^{L} G_{1,2}^{2,1}\left(\frac{s}{A_\ell}\middle| \begin{matrix}1-m_\ell \\ 0, m_{s_\ell}\end{matrix}\right), \end{aligned} \quad \text{(A-4)}$$

where $\zeta_0 = 0$, $\mathcal{L}_\ell$ $(\ell = 1, \ldots, L)$ goes from $\sigma_\ell - \infty j$ to $\sigma_\ell + \infty j$, $\sigma_\ell \in \mathbb{R}$ and $\Upsilon(\zeta_\ell) \triangleq \Gamma(m_\ell + \zeta_{\ell-1} - \zeta_\ell)\Gamma(-\zeta_{\ell-1} + \zeta_\ell)\Gamma(m_{s_\ell} - \zeta_{\ell-1} + \zeta_\ell)$. Using [46, eq. (07.34.16.0001.01)] and rewriting each Meijer's G-function as a Mellin-Barnes integral, we express (A-4) as

$$I_G = \left(\frac{1}{2\pi j}\right)^L \int_{\mathcal{L}_1}\cdots\int_{\mathcal{L}_L} \prod_{\ell=1}^{L}\Upsilon(\zeta_\ell) \times \prod_{\ell=1}^{L}\left(\frac{A_\ell}{A_{\ell+1}}\right)^{\zeta_\ell}\left(\frac{1}{s}\right)^{\zeta_L} d\zeta_1\cdots d\zeta_L. \quad \text{(A-5)}$$

Substituting (A-5) into (A-3), we obtain

$$f_z(z) = \left(\frac{1}{2\pi j}\right)^L \prod_{\ell=1}^{L}\frac{1}{\Gamma(m_{s_\ell})\Gamma(m_\ell)} \int_{\mathcal{L}_1}\cdots\int_{\mathcal{L}_L}\prod_{\ell=1}^{L}\Upsilon(\zeta_\ell) \times \prod_{\ell=1}^{L}\left(\frac{A_\ell}{A_{\ell+1}}\right)^{\zeta_\ell} \underbrace{\frac{1}{2\pi j}\int_{\mathcal{L}} s^{-\zeta_L}e^{zs}ds}_{I_A} d\zeta_1\cdots d\zeta_L. \quad \text{(A-6)}$$

Using [30, eq. (8.315.1)], we can solve I_A as

$$I_A = \frac{z^{-1+\zeta_L}}{\Gamma(\zeta_L)}. \quad \text{(A-7)}$$

Substituting (A-7) into (A-6), we can write (A-6) as

$$f_z(z) = \left(\frac{1}{2\pi j}\right)^L \prod_{\ell=1}^{L}\frac{1}{z\Gamma(m_{s_\ell})\Gamma(m_\ell)} \times \int_{\mathcal{L}_1}\cdots\int_{\mathcal{L}_L}\frac{\prod_{\ell=1}^{L}\Upsilon(\zeta_\ell)}{\Gamma(\zeta_L)}\prod_{\ell=1}^{L}\left(\frac{A_\ell}{A_{\ell+1}}\right)^{\zeta_\ell} z^{\zeta_L}d\zeta_1\cdots d\zeta_L. \quad \text{(A-8)}$$

The proof is completed by deriving (9) using the definition of the multivariate H-function [31, eq. (A.1)].

APPENDIX B
PROOF OF THEOREM 3

The parameters of the proposed distributions can be obtained in a straightforward manner by employing a simple moment matching technique. Let us start with $L = 2$ and $z = \gamma_1 + \gamma_2$, $z \sim \mathcal{F}(\overline{\gamma}, m, m_s)$ and $\gamma_\ell \sim \mathcal{F}(\overline{\gamma}_\ell, m_\ell, m_{s_\ell})$ $(\ell = 1, 2)$. The first, second and third moments of the sum of two independent RVs can be written as

$$\begin{cases} \mathrm{E}[z] = \mathrm{E}[\gamma_1] + \mathrm{E}[\gamma_2], \\ \mathrm{E}\big[z^2\big] = \mathrm{E}\big[\gamma_1^2\big] + \mathrm{E}\big[\gamma_2^2\big] + 2\mathrm{E}\big[\gamma_1\big]\mathrm{E}\big[\gamma_2\big], \\ \mathrm{E}\big[z^3\big] = \mathrm{E}\big[\gamma_1^3\big] + \mathrm{E}\big[\gamma_2^3\big] + 3\mathrm{E}\big[\gamma_1^2\big]\mathrm{E}\big[\gamma_2\big] + 3\mathrm{E}\big[\gamma_1\big]\mathrm{E}\big[\gamma_2^2\big]. \end{cases} \tag{B-1}$$

With the help of (5) and the moment matching method, eq. (B-1) can be written as

$$\begin{cases} \bar{\gamma}_{\mathcal{F}} = \bar{\gamma}_1 + \bar{\gamma}_2, \\ H_{\mathcal{F}} \bar{\gamma}^2 = H_1 \bar{\gamma}_1^2 + H_2 \bar{\gamma}_2^2 + 2\bar{\gamma}_1 \bar{\gamma}_2, \\ H_{\mathcal{F}} Y_{\mathcal{F}} \bar{\gamma}^3 = H_1 Y_1 \bar{\gamma}_1^3 + H_2 Y_2 \bar{\gamma}_2^3 + 3H_1 \bar{\gamma}_1^2 \bar{\gamma}_2 + 3H_2 \bar{\gamma}_1 \bar{\gamma}_2^2, \end{cases} \tag{B-2}$$

where $H_{\mathcal{F}} = \frac{(1+m)(m_s-1)}{m(m_s-2)}$, $Y_{\mathcal{F}} = \frac{(m_s-1)(2+m)}{m(m_s-3)}$, $H_\ell = \frac{(1+m_\ell)(m_{s_\ell}-1)}{m_\ell(m_{s_\ell}-2)}$, $Y_\ell = \frac{(m_{s_\ell}-1)(2+m_\ell)}{m_\ell(m_{s_\ell}-3)}$ $(\ell = 1, 2)$. In the composite fading channel, an $\mathcal{F}$ fading channel's amount of fading (AF), which is often used as a relative measure of the severity of fading, is derived in [1] as $(H_{\mathcal{F}} - 1)$. By solving (B-2), we obtain

$$\begin{cases} \bar{\gamma}_{\mathcal{F}} = \bar{\gamma}_1 + \bar{\gamma}_2, \\ H_{\mathcal{F}} = \frac{H_1\bar{\gamma}_1^2 + H_2\bar{\gamma}_2^2 + 2\bar{\gamma}_1\bar{\gamma}_2}{(\bar{\gamma}_1+\bar{\gamma}_2)^2} = \frac{(H_1-1)\bar{\gamma}_1^2 + (H_2-1)\bar{\gamma}_2^2}{(\bar{\gamma}_1+\bar{\gamma}_2)^2} + 1, \\ Y_{\mathcal{F}} = \frac{H_1Y_1\bar{\gamma}_1^3 + H_2Y_2\bar{\gamma}_2^3 + 3\bar{\gamma}_1^2\bar{\gamma}_2 H_1 + 3\bar{\gamma}_1\bar{\gamma}_2^2 H_2}{(\bar{\gamma}_1+\bar{\gamma}_2)\big(H_1\bar{\gamma}_1^2 + H_2\bar{\gamma}_2^2 + 2\bar{\gamma}_1\bar{\gamma}_2\big)} \\ \quad = \frac{(H_1Y_1-1)\bar{\gamma}_1^3 + (H_2Y_2-1)\bar{\gamma}_2^3 + (\bar{\gamma}_1+\bar{\gamma}_2)^3 - 3\big(\bar{\gamma}_1^3(H_1-1) + \bar{\gamma}_2^3(H_2-1)\big)}{(\bar{\gamma}_1+\bar{\gamma}_2)\big((H_1-1)\bar{\gamma}_1^2 + (H_2-1)\bar{\gamma}_2^2 + (\bar{\gamma}_1+\bar{\gamma}_2)^2\big)} \\ \qquad + \frac{3\big(\bar{\gamma}_1^2(H_1-1) + \bar{\gamma}_2^2(H_2-1)\big)}{\big((H_1-1)\bar{\gamma}_1^2 + (H_2-1)\bar{\gamma}_2^2 + (\bar{\gamma}_1+\bar{\gamma}_2)^2\big)} \end{cases} \tag{B-3}$$

Equations (B-3) can be generalized for the sum of L i.n.i.d. Fisher-Snedecor $\mathcal{F}$ RVs as [47]

$$\begin{cases} \bar{\gamma}_{\mathcal{F}} = \sum_{\ell=1}^{L} \bar{\gamma}_\ell, \\ H_{\mathcal{F}} = \frac{\sum_{\ell=1}^{L} (H_\ell - 1)\bar{\gamma}_\ell^2}{\left(\sum_{\ell=1}^{L} \bar{\gamma}_\ell\right)^2} + 1, \\ Y_F = \frac{\sum_{\ell=1}^{L} (H_\ell Y_\ell - 1)\bar{\gamma}_\ell^3 + \left(\sum_{\ell=1}^{L} \bar{\gamma}_\ell\right)^3 - 3\sum_{\ell=1}^{L} (H_\ell - 1)\bar{\gamma}_\ell^3}{\left(\sum_{\ell=1}^{L} \bar{\gamma}_\ell\right)\left(\sum_{\ell=1}^{L} (H_\ell - 1)\bar{\gamma}_\ell^2 + \left(\sum_{\ell=1}^{L} \bar{\gamma}_\ell\right)^2\right)} \\ \qquad + \frac{3\left(\sum_{\ell=1}^{L} (H_\ell - 1)\bar{\gamma}_\ell^2\right)}{\left(\sum_{\ell=1}^{L} (H_\ell - 1)\bar{\gamma}_\ell^2 + \left(\sum_{\ell=1}^{L} \bar{\gamma}_\ell\right)^2\right)} \end{cases} \tag{B-4}$$

However, the parameters of a single $\mathcal{F}$ distribution calculated by (B-4) result in a relatively large approximation error in the lower and upper tail regions because we only match the first, second and third moments. This error can be modified by introducing an adjustment factor ε. The proof is completed by deriving (14) and (15).

APPENDIX C
PROOF FOR PROPOSITION 2

Using the classical Newton-Leibniz formula, we can rewrite (22) as

$$\begin{aligned} C_{\text{eff}} &= -\frac{1}{A}\log_2\left(\int_0^\infty \frac{1}{(1+z)^A} f_z(z)dz\right) \\ &= -\frac{1}{A}\log_2\left(A\underbrace{\int_0^\infty \frac{F_z(z)}{(1+z)^{A+1}}dz}_{I_1}\right). \end{aligned} \tag{C-1}$$

With the help of (12), I_1 can be expressed as

$$\begin{aligned} I_1 = &\prod_{\ell=1}^{L} \frac{1}{\Gamma(m_\ell)\Gamma\big(m_{s_\ell}\big)}\left(\frac{1}{2\pi j}\right)^L \\ &\times \int_0^\infty \frac{1}{(1+z)^{A+1}} \int_{\mathcal{L}_1}\int_{\mathcal{L}_2}\cdots\int_{\mathcal{L}_L} \frac{1}{\Gamma(1+\zeta_\ell)} \\ &\times \prod_{\ell=1}^{L} \Upsilon(\zeta_\ell)\left(\frac{A_\ell}{A_{\ell+1}}\right)^{\zeta_\ell} z^{\zeta_L} d\zeta_1 d\zeta_2 \cdots d\zeta_L dz. \end{aligned} \tag{C-2}$$

According to Fubini's theorem, we can exchange the order of integration in I_1, and derive

$$\begin{aligned} I_1 = &\prod_{\ell=1}^{L} \frac{1}{\Gamma(m_\ell)\Gamma\big(m_{s_\ell}\big)}\left(\frac{1}{2\pi j}\right)^L \\ &\times \int_{\mathcal{L}_1}\int_{\mathcal{L}_2}\cdots\int_{\mathcal{L}_L} \frac{1}{\Gamma(1+\zeta_L)} \prod_{\ell=1}^{L} \Upsilon(\zeta_\ell)\left(\frac{A_\ell}{A_{\ell+1}}\right)^{\zeta_\ell} \\ &\times \underbrace{\int_0^\infty \frac{z^{\zeta_L}}{(1+z)^{A+1}}dz}_{I_2} d\zeta_1 d\zeta_2 \cdots d\zeta_L. \end{aligned} \tag{C-3}$$

Using [30, eq. (3.194.3)], we can solve I_2 as

$$I_2 = \frac{\Gamma(\zeta_L)\Gamma(A-\zeta_L)}{\Gamma(1+A)}. \tag{C-4}$$

We complete the proof combining (C-4), (C-3), (C-1) and (6).

APPENDIX D
PROOF FOR PROPOSITION 3

With the aid of (9), the integral in (26) can be written as

$$\begin{aligned} I_3 = &\prod_{\ell=1}^{L} \frac{1}{\Gamma\big(m_{s_\ell}\big)\Gamma(m_\ell)}\left(\frac{1}{2\pi j}\right)^L \\ &\times \int_0^\infty \int_{\mathcal{L}_1}\int_{\mathcal{L}_2}\cdots\int_{\mathcal{L}_L} \prod_{\ell=1}^{L} \Upsilon(\zeta_\ell)\left(\frac{A_\ell}{A_{\ell+1}}\right)^{\zeta_\ell} \\ &\times \frac{1}{\Gamma(\zeta_L)} z^{-2+\zeta_L} d\zeta_1 d\zeta_2 \cdots d\zeta_L dz. \end{aligned} \tag{D-1}$$

Let $\mathcal{L}\{p(t)\} = P(x)$. According to the property of Laplace transform, we have

$$\mathcal{L}\left\{\int_0^t p(z)dz\right\} = \frac{P(x)}{x}. \tag{D-2}$$

With the help of the final value theorem, it follows that

$$\lim_{t\to\infty}\left(\int_0^t p(z)dz\right)=s\frac{P(s)}{s}=P(s). \tag{D-3}$$

We can use (D-3) to obtain

$$\int_0^\infty z^{-2+\zeta_L}dz=\mathcal{L}\left\{z^{-2+\zeta_L}\right\}=\left(\frac{1}{s}\right)^{\zeta_L-1}\Gamma(\zeta_L-1). \tag{D-4}$$

Employing (D-1) and (D-4), we can rewrite I_3 as

$$I_3=\prod_{\ell=1}^{L}\frac{s}{\Gamma(m_{s_\ell})\Gamma(m_\ell)}\left(\frac{1}{2\pi j}\right)^L\int_{\mathcal{L}_1}\int_{\mathcal{L}_2}\cdots\int_{\mathcal{L}_L}\frac{\Gamma(\zeta_L-1)}{\Gamma(\zeta_L)}\times\prod_{\ell=1}^{L}\Upsilon(\zeta_\ell)\left(\frac{A_\ell}{sA_{\ell+1}}\right)^{\zeta_\ell}d\zeta_1d\zeta_2\cdots d\zeta_L. \tag{D-5}$$

Substituting (D-5) into (26) and using (6), we obtain (27) which completes the proof.

APPENDIX E
PROOF FOR PROPOSITION 4

Observe that

$$\int_{z_0}^\infty f_Z(z)dz=1-\int_0^{z_0}f_Z(z)dz=1-F_Z(z_0), \tag{D-1}$$

where $F_Z(z_0)$ can be deduced using (12). Thus, C_{TIFR} can be expressed as

$$C_{\text{TIFR}}=B\log_2\left(1+\frac{1}{\underbrace{\int_{z_0}^\infty\frac{f_Z(z)}{z}dz}_{I_5}}\right)\times\left(1-\prod_{\ell=1}^{L}\frac{1}{\Gamma(m_{s_\ell})\Gamma(m_\ell)}H_{CDF}\right). \tag{D-2}$$

Substituting (9) into (D-2), we can rewrite I_5 as

$$I_5=\prod_{\ell=1}^{L}\frac{1}{\Gamma(m_{s_\ell})\Gamma(m_\ell)}\left(\frac{1}{2\pi j}\right)^L\times\int_{z_0}^\infty\int_{\mathcal{L}_1}\int_{\mathcal{L}_2}\cdots\int_{\mathcal{L}_L}\frac{1}{\Gamma(\zeta_L)}\prod_{\ell=1}^{L}\Upsilon(\zeta_\ell)\left(\frac{A_\ell}{A_{\ell+1}}\right)^{\zeta_\ell}\times z^{-2+\zeta_L}d\zeta_1d\zeta_2\cdots d\zeta_Ldz. \tag{D-3}$$

Note that the order of integration can be interchangeable according to Fubini's theorem. Thus, we can express I_5 as

$$I_5=\prod_{\ell=1}^{L}\frac{1}{\Gamma(m_{s_\ell})\Gamma(m_\ell)}\left(\frac{1}{2\pi j}\right)^L\times\int_{\mathcal{L}_1}\int_{\mathcal{L}_2}\cdots\int_{\mathcal{L}_L}\frac{\Gamma(1-\zeta_L)}{\Gamma(\zeta_L)\Gamma(2-\zeta_L)}\times\prod_{\ell=1}^{L}\Upsilon(\zeta_\ell)\left(\frac{z_0A_\ell}{A_{\ell+1}}\right)^{\zeta_\ell}d\zeta_1d\zeta_2\cdots d\zeta_L. \tag{D-4}$$

Employing (6) and substituting (D-4) into (D-2), we obtain (30) to complete the proof.

APPENDIX F
PROOF FOR PROPOSITION 5

Substituting (9) into (32) and changing the order of integration, the channel capacity under ORA can be expressed as

$$C_{\text{ORA}}=B\prod_{\ell=1}^{L}\frac{1}{\Gamma(m_{s_\ell})\Gamma(m_\ell)}\left(\frac{1}{2\pi j}\right)^L\int_{\mathcal{L}_1}\times\int_{\mathcal{L}_2}\cdots\int_{\mathcal{L}_L}\frac{1}{\Gamma(\zeta_L)}\prod_{\ell=1}^{L}\Upsilon(\zeta_\ell)\left(\frac{A_\ell}{A_{\ell+1}}\right)^{\zeta_\ell}\times\underbrace{\int_0^\infty\log_2(1+z)z^{-1+\zeta_L}dz}_{I_6}d\zeta_1d\zeta_2\cdots d\zeta_L. \tag{D-1}$$

With the help of [48, eq. (2.6.9.21)] and [30, eq. (8.334.3)], I_6 can be deduced as

$$I_6=\int_0^\infty\log_2(1+z)z^{-1+\zeta_L}d\gamma=-\frac{1}{\ln 2}\Gamma(\zeta_L)\Gamma(-\zeta_L), \tag{D-2}$$

where $-1<\mathbb{R}(\zeta_L)<0$.

To avoid potential conflicts with the definition of the multivariate H-function, employing [49, eq. (2.5.16)], we can express I_6 as

$$I_6=\frac{1}{\ln(2)}\int_0^\infty G_{2,2}^{1,2}\left(z\middle|\begin{matrix}\zeta_L,\zeta_L\\ \zeta_L,\zeta_L-1\end{matrix}\right)dz. \tag{D-3}$$

Using [30, eq. (9.301)] and the Laplace transform of Meijer's G-function [46, eq. (07.34.22.0003.01)], we obtain

$$\mathcal{L}\left\{G_{2,2}^{1,2}\left(z\middle|\begin{matrix}\zeta_L,\zeta_L\\ \zeta_L,\zeta_L-1\end{matrix}\right)\right\}=\frac{1}{x}G_{3,2}^{1,3}\left(\frac{1}{x}\middle|\begin{matrix}0,\zeta_L,\zeta_L\\ \zeta_L,\zeta_L-1\end{matrix}\right)=\int_{\mathcal{L}_{L+1}}\frac{\Gamma(1-\zeta_{L+1})\Gamma^2(1-\zeta_L-\zeta_{L+1})\Gamma(\zeta_L+\zeta_{L+1})}{\Gamma(2-\zeta_L-\zeta_{L+1})}\times x^{\zeta_{L+1}}\,d\zeta_{L+1}. \tag{D-4}$$

Thus, using the final value theorem and following the similar procedures as the proof of (27), we can rewrite the channel capacity under ORA as

$$C_{\text{ORA}}=\frac{B}{s\ln(2)}\prod_{\ell=1}^{L}\frac{1}{\Gamma(m_{s_\ell})\Gamma(m_\ell)}\left(\frac{1}{2\pi i}\right)^{L+1}\times\int_{\mathcal{L}_1}\int_{\mathcal{L}_2}\cdots\int_{\mathcal{L}_{L+1}}\frac{\Gamma^2(1-\zeta_L-\zeta_{L+1})\Gamma(\zeta_L+\zeta_{L+1})}{\Gamma(2-\zeta_L-\zeta_{L+1})\Gamma(\zeta_L)}\times\prod_{\ell=1}^{L}\Upsilon(\zeta_\ell)\left(\frac{A_\ell}{A_{\ell+1}}\right)^{\zeta_\ell}\times\frac{\Gamma(1-\zeta_{L+1})\Gamma(\zeta_{L+1})}{\Gamma(\zeta_{L+1}+1)}s^{\zeta_{L+1}}d\zeta_1d\zeta_2\cdots d\zeta_{L+1}. \tag{D-5}$$

Equation (33) is obtained using (D-5) and (6), and the proof is complete.

APPENDIX G
PROOF FOR PROPOSITION 6

Substituting (9) into (35) and changing the order of integration, we can rewrite the channel capacity under OPRA as

$$\begin{aligned} C_{\text{OPRA}} &= \prod_{\ell=1}^{L} \frac{1}{\Gamma(m_\ell)\Gamma\left(m_{s_\ell}\right)} \left(\frac{1}{2\pi j}\right)^L \int_{\mathcal{L}_1} \\ &\times \int_{\mathcal{L}_2} \cdots \int_{\mathcal{L}_L} \frac{1}{\Gamma(\zeta_L)} \prod_{\ell=1}^{L} \Upsilon(\zeta_\ell) \left(\frac{A_\ell}{A_{\ell+1}}\right)^{\zeta_\ell} \\ &\times \underbrace{\int_{\gamma_0}^{\infty} \log_2\left(\frac{z}{\gamma_0}\right) z^{-1+\zeta_L} dz}_{I_7} d\zeta_1 d\zeta_2 \cdots d\zeta_L. \end{aligned} \tag{D-1}$$

Let $t = z/\gamma_0 - 1$ and we have

$$I_7 = {\gamma_0}^{\zeta_L} \int_0^{\infty} \log_2(t+1)(t+1)^{-1+\zeta_L} dt. \tag{D-2}$$

Using [48, eq. (2.6.10.49)], [48, eq. (II.2)] and [30, eq. (8.331.1)], we can solve I_7 as

$$I_7 = \frac{1}{\ln 2} \frac{\Gamma(-\zeta_L)\Gamma(-\zeta_L){\gamma_0}^{\zeta_L}}{\Gamma(1-\zeta_L)\Gamma(1-\zeta_L)}. \tag{D-3}$$

However, eq. (D-3) has conflict with the definition of the multivariate 's H-function; therefore, we choose another way to solve I_7. Using the final value theorem and following the similar procedures as the proof of (27), we can rewrite I_7 as

$$I_7 = \frac{1}{2\pi j} {\gamma_0}^{\zeta_L} \int_{\mathcal{L}_{L+1}} \frac{\Gamma^2(-\zeta_L - \zeta_{L+1}\zeta_\ell)\Gamma(-\zeta_{L+1})}{\Gamma^2(1 - -\zeta_L - \zeta_{L+1}\zeta_\ell)} s^{\zeta_{L+1}} d\zeta_{L+1}. \tag{D-4}$$

Substituting (D-4) into (D-1), we obtain

$$\begin{aligned} C_{\text{OPRA}} &= \prod_{\ell=1}^{L} \frac{1}{\Gamma(m_\ell)\Gamma\left(m_{s_\ell}\right)} \left(\frac{1}{2\pi j}\right)^{L+1} \\ &\times \int_{\mathcal{L}_1} \int_{\mathcal{L}_2} \cdots \int_{\mathcal{L}_{L+1}} \frac{\Gamma^2(-\zeta_L - \zeta_{L+1})}{\Gamma(\zeta_L)\Gamma^2(1-\zeta_L-\zeta_{L+1})} s^{\zeta_{L+1}} \\ &\times \prod_{\ell=1}^{L} \Upsilon(\zeta_\ell) \left(\frac{\gamma_0 A_\ell}{A_{\ell+1}}\right)^{\zeta_\ell} \Gamma(-\zeta_{L+1}) d\zeta_1 d\zeta_2 \cdots d\zeta_{L+1}. \end{aligned} \tag{D-5}$$

With the help of (6), we obtain (39). The proof is now complete.

REFERENCES

[1] S. K. Yoo, S. L. Cotton, P. C. Sofotasios, M. Matthaiou, M. Valkama, and G. K. Karagiannidis, "The Fisher–Snedecor $\mathcal{F}$ distribution: A simple and accurate composite fading model," *IEEE Commun. Lett.*, vol. 21, no. 7, pp. 1661–1664, Jul. 2017.

[2] J. Zhang, L. Dai, Z. He, S. Jin, and X. Li, "Performance analysis of mixed-ADC massive MIMO systems over Rician fading channels," *IEEE J. Sel. Areas Commun.*, vol. 35, no. 6, pp. 1327–1338, Jun. 2017.

[3] J. Zhang, L. Dai, S. Sun, and Z. Wang, "On the spectral efficiency of massive MIMO systems with low-resolution ADCs," *IEEE Commun. Lett.*, vol. 20, no. 5, pp. 842–845, Feb. 2016.

[4] Ö. Özdogan, E. Björnson, and J. Zhang, "Performance of cell-free massive MIMO with Rician fading and phase shifts," *IEEE Trans. Wireless Commun.*, vol. 18, no. 11, pp. 5299–5315, Nov. 2019.

[5] J. Zhang, M. Matthaiou, Z. Tan, and H. Wang, "Performance analysis of digital communication systems over composite η-μ/gamma fading channels," *IEEE Trans. Veh. Technol.*, vol. 61, no. 7, pp. 3114–3124, Sep. 2012.

[6] L. Kong and G. Kaddoum, "On physical layer security over the Fisher–Snedecor $\mathcal{F}$ wiretap fading channels," *IEEE Access*, vol. 6, pp. 39466–39472, 2018.

[7] N. Kapucu and M. Bilim, "Analysis of analytical capacity for Fisher–Snedecor $\mathcal{F}$ fading channels with different transmission schemes," *Electron. Lett.*, vol. 55, no. 5, pp. 283–285, May 2019.

[8] S. K. Yoo, P. C. Sofotasios, S. L. Cotton, S. Muhaidat, O. S. Badarneh, and G. K. Karagiannidis, "Entropy and energy detection-based spectrum sensing over $\mathcal{F}$ composite fading channels," *IEEE Trans. Commun.*, vol. 67, no. 7, pp. 4641–4653, Jul. 2019.

[9] H. Zhao, L. Yang, A. S. Salem, and M.-S. Alouini, "Ergodic capacity under power adaption over Fisher–Snedecor $\mathcal{F}$ fading channels," *IEEE Commun. Lett.*, vol. 23, no. 3, pp. 546–549, Mar. 2019.

[10] H. Du, J. Zhang, K. P. Peppas, H. Zhao, B. Ai, and X. Zhang, "On the distribution of the ratio of products of Fisher–Snedecor $\mathcal{F}$ random variables and its applications," *IEEE Trans. Veh. Technol.*, vol. 69, no. 2, pp. 1855–1866, Feb. 2020.

[11] P. Zhang, J. Zhang, K. P. Peppas, D. W. K. Ng, and B. Ai, "Dual-hop relaying communications over Fisher–Snedecor $\mathcal{F}$-fading channels," *IEEE Trans. Commun.*, early access, Feb. 11, 2020, doi: 10.1109/TCOMM.2020.2973263.

[12] M. K. Simon and M.-S. Alouini, *Digital Communication Over Fading Channels*. Hoboken, NJ, USA: Wiley, 2005.

[13] S. Chen, J. Zhang, G. K. Karagiannidis, and B. Ai, "Effective rate of MISO systems over Fisher–Snedecor $\mathcal{F}$ fading channels," *IEEE Commun. Lett.*, vol. 22, no. 12, pp. 2619–2622, Dec. 2018.

[14] F. El Bouanani and D. B. da Costa, "Accurate closed-form approximations for the sum of correlated Weibull random variables," *IEEE Wireless Commun. Lett.*, vol. 7, no. 4, pp. 498–501, Aug. 2018.

[15] J. Zhang, L. Dai, Y. Han, Y. Zhang, and Z. Wang, "On the ergodic capacity of MIMO free-space optical systems over turbulence channels," *IEEE J. Sel. Areas Commun.*, vol. 33, no. 9, pp. 1925–1934, Sep. 2015.

[16] K. Peppas, F. Lazarakis, A. Alexandridis, and K. Dangakis, "Error performance of digital modulation schemes with MRC diversity reception over η–μ fading channels," *IEEE Trans. Wireless Commun.*, vol. 8, no. 10, pp. 4974–4980, Oct. 2009.

[17] J. Zheng, J. Zhang, G. Pan, J. Cheng, and B. Ai, "Sum of squared fluctuating two-ray random variables with wireless applications," *IEEE Trans. Veh. Technol.*, vol. 68, no. 8, pp. 8173–8177, Aug. 2019.

[18] J. Zhang, X. Chen, K. P. Peppas, X. Li, and Y. Liu, "On high-order capacity statistics of spectrum aggregation systems over κ–μ and κ–μ shadowed fading channels," *IEEE Trans. Commun.*, vol. 65, no. 2, pp. 935–944, Feb. 2017.

[19] J. D. V. Sánchez, L. Urquiza-Aguiar, and M. C. P. Paredes, "An accurate, fast approximation for the sum of fading random variables via expectation maximization applications to diversity systems," *IEEE Access*, vol. 6, pp. 42616–42630, 2018.

[20] K. P. Peppas, G. P. Efthymoglou, and A. G. Kanatas, "Approximations to the distribution of the sum of generalized normal RVs using the moments matching method and its applications in performance analysis of equal gain diversity receivers," *IEEE Trans. Veh. Technol.*, vol. 67, no. 8, pp. 7230–7241, Aug. 2018.

[21] V. Perim, J. D. V. Sánchez, and J. C. S. S. Filho, "Asymptotically exact approximations to generalized fading sum statistics," *IEEE Trans. Wireless Commun.*, vol. 19, no. 1, pp. 205–217, Oct. 2019.

[22] J. Zhang, M. Matthaiou, G. K. Karagiannidis, H. Wang, and Z. Tan, "Gallager's exponent analysis of STBC MIMO systems over η–μ and κ–μ fading channels," *IEEE Trans. Commun.*, vol. 61, no. 3, pp. 1028–1039, Mar. 2013.

[23] O. S. Badarneh, D. B. da Costa, P. C. Sofotasios, S. Muhaidat, and S. L. Cotton, "On the sum of Fisher–Snedecor $\mathcal{F}$ variates and its application to maximal-ratio combining," *IEEE Wireless Commun. Lett.*, vol. 7, no. 6, pp. 966–969, Dec. 2018.

[24] Y. A. Rahama, M. H. Ismail, and M. S. Hassan, "On the sum of independent Fox's h-function variates with applications," *IEEE Trans. Veh. Technol.*, vol. 67, no. 8, pp. 6752–6760, Aug. 2018.

[25] J. D. V. Sánchez, D. P. M. Osorio, E. E. B. Olivo, H. Alves, M. C. P. Paredes, and L. U. Aguiar, "On the statistics of the ratio of nonconstrained arbitrary α–μ random variables: A general framework and applications," *Trans. Emerg. Telcommun. Technol.*, Feb. 2019, Art. no. e3832.
[26] H. Chergui, M. Benjillali, and M.-S. Alouini, "Rician K-factor-based analysis of XLOS service probability in 5G outdoor ultra-dense networks," *IEEE Wireless Commun. Lett.*, vol. 8, no. 2, pp. 428–431, Apr. 2018.
[27] C. R. N. Da Silva, N. Simmons, E. J. Leonardo, S. L. Cotton, and M. D. Yacoub, "Ratio of two envelopes taken from α–μ, η–μ, and κ–μ variates and some practical applications," *IEEE Access*, vol. 7, pp. 54449–54463, May 2019.
[28] H. R. Alhennawi, M. M. El Ayadi, M. H. Ismail, and H.-A. M. Mourad, "Closed-form exact and asymptotic expressions for the symbol error rate and capacity of the h-function fading channel," *IEEE Trans. Veh. Technol.*, vol. 65, no. 4, pp. 1957–1974, Apr. 2015.
[29] S. K. Yoo *et al.*, "A comprehensive analysis of the achievable channel capacity in $\mathcal{F}$ composite fading channels," *IEEE Access*, vol. 7, pp. 34078–34094, 2019.
[30] I. S. Gradshteyn and I. M. Ryzhik, *Table of Integrals, Series, and Products*, 7th ed. Burlington, MA, USA: Academic, 2007.
[31] A. Mathai, R. K. Saxena, and H. Haubold, *The H-Function: Theory and Applications*. New York, NY, USA: Springer-Verlag, 2010.
[32] A. Papoulis and S. U. Pillai, *Probability, Random Variables, and Stochastic Processes*. Boston, MA, USA: McGraw-Hill, 2002.
[33] J. Zhang, M. Matthaiou, G. K. Karagiannidis, and L. Dai, "On the multivariate gamma–gamma distribution with arbitrary correlation and applications in wireless communications," *IEEE Trans. Veh. Technol.*, vol. 65, no. 5, pp. 3834–3840, May 2016.
[34] J. Zhang, Z. Tan, H. Wang, Q. Huang, and L. Hanzo, "The effective throughput of MISO systems over κ–μ fading channels," *IEEE Trans. Veh. Technol.*, vol. 63, no. 2, pp. 943–947, Feb. 2013.
[35] J. Zhang, L. Dai, W. H. Gerstacker, and Z. Wang, "Effective capacity of communication systems over κ–μ shadowed fading channels," *Electron. Lett.*, vol. 51, no. 19, pp. 1540–1542, Sep. 2015.
[36] M. You, H. Sun, J. Jiang, and J. Zhang, "Unified framework for the effective rate analysis of wireless communication systems over MISO fading channels," *IEEE Trans. Commun.*, vol. 65, no. 4, pp. 1775–1785, Apr. 2016.
[37] J. Zhang, L. Dai, Z. Wang, D. W. K. Ng, and W. H. Gerstacker, "Effective rate analysis of MISO systems over α–μ fading channels," in *Proc. IEEE Global Commun. (Globecom)*, Dec. 2015, pp. 1–6.
[38] J. Zhang, M. Matthaiou, Z. Tan, and H. Wang, "Effective rate analysis of MISO η–μ fading channels," in *Proc. IEEE Int. Conf. Commun. (ICC)*, Jun. 2013, pp. 5840–5844.
[39] M. C. Gursoy, D. Qiao, and S. Velipasalar, "Analysis of energy efficiency in fading channels under QoS constraints," *IEEE Trans. Wireless Commun.*, vol. 8, no. 8, pp. 4252–4263, Aug. 2009.
[40] M.-S. Alouini and A. J. Goldsmith, "Capacity of Rayleigh fading channels under different adaptive transmission and diversity-combining techniques," *IEEE Trans. Veh. Technol.*, vol. 48, no. 4, pp. 1165–1181, Apr. 1999.
[41] A. J. Goldsmith and P. P. Varaiya, "Capacity of fading channels with channel side information," *IEEE Trans. Inf. Theory*, vol. 43, no. 6, pp. 1986–1992, Nov. 1997.
[42] J. Cheng and T. Berger, "Capacity of a class of fading channels with channel state information (CSI) feedback," in *Proc. Allerton Conf. Commun. Control Comput.*, Oct. 2001, pp. 1152–1160.
[43] A. Goldsmith, *Wireless Communications*. Cambridge, U.K.: Cambridge Univ. Press, 2005.
[44] M.-S. Alouini and A. J. Goldsmith, "Comparison of fading channel capacity under different CSI assumptions," in *Proc. IEEE Veh. Technol. Conf.*, Sep. 2000, pp. 1844–1849.
[45] A. P. Prudnikov, J. A. Bryčkov, and O. I. Maričev, *Integrals and Series*, vol. 3. New York, NY, USA: Gordon and Breach, 2003.
[46] Wolfram. (Apr. 2020). *The Wolfram Functions Site*. [Online]. Available: http://functions.wolfram.com
[47] S. Al-Ahmadi and H. Yanikomeroglu, "On the approximation of the generalized-K distribution by a gamma distribution for modeling composite fading channels," *IEEE Trans. Wireless Commun.*, vol. 9, no. 2, pp. 706–713, Feb. 2010.
[48] A. P. Prudnikov, J. A. Bryčkov, and O. I. Maričev, *Integrals and Series*, vol. 1. New York, NY, USA: Gordon and Breach, 1986.
[49] A. Kilbas and M. Saigo, *H-Transforms: Theory and Applications. Analytical Methods and Special Functions*. Boca Raton, FL, USA: CRC Press, 2004.

HONGYANG DU is currently pursuing the bachelor's degree in communications engineering with Beijing Jiaotong University, Beijing, China. His research interests include large intelligent surface and digital communications over generalized fading channels.

JIAYI ZHANG (Member, IEEE) received the B.Sc. and Ph.D. degrees in communication engineering from Beijing Jiaotong University, China, in 2007 and 2014, respectively.

Since 2016, he has been a Professor with the School of Electronic and Information Engineering, Beijing Jiaotong University. From 2014 to 2016, he was a Postdoctoral Research Associate with the Department of Electronic Engineering, Tsinghua University, China. From 2014 to 2015, he was also a Humboldt Research Fellow with the Institute for Digital Communications, Friedrich–Alexander-University Erlangen–Nürnberg, Germany. From 2012 to 2013, he was a Visiting Scholar with the Wireless Group, University of Southampton, U.K. His current research interests include massive MIMO, large intelligent surface, communication theory, and applied mathematics. He received the Best Paper Awards at WCSP 2017 and IEEE APCC 2017. He was recognized as an Exemplary Reviewer of IEEE COMMUNICATIONS LETTERS in 2015 and 2016. He was also recognized as an Exemplary Reviewer of the IEEE TRANSACTIONS ON COMMUNICATIONS in 2017. He was the Lead Guest Editor of the Special Issue on Multiple Antenna Technologies for Beyond 5G of the IEEE JOURNAL ON SELECTED AREAS IN COMMUNICATIONS. He currently serves as an Associate Editor for the IEEE TRANSACTIONS ON COMMUNICATIONS, IEEE COMMUNICATIONS LETTERS, IEEE ACCESS, and *IET Communications*.

JULIAN CHENG (Senior Member, IEEE) received the B.Eng. degree (Hons.) in electrical engineering from the University of Victoria, Victoria, BC, Canada, in 1995, the M.Sc.(Eng.) degree in mathematics and engineering from Queens University, Kingston, ON, Canada, in 1997, and the Ph.D. degree in electrical engineering from the University of Alberta, Edmonton, AB, Canada, in 2003. He is currently a Full Professor with the School of Engineering, Faculty of Applied Science, University of British Columbia, Kelowna, BC, Canada. He was with Bell Northern Research and NORTEL Networks. His current research interests include digital communications over fading channels, statistical signal processing for wireless applications, optical wireless communications, and 5G wireless networks. He was the Co-Chair of the 12th Canadian Workshop on Information Theory in 2011, the 28th Biennial Symposium on Communications in 2016, and the 6th EAI International Conference on Game Theory for Networks (GameNets 216). He currently serves as an Area Editor for the IEEE TRANSACTIONS ON COMMUNICATIONS. He was an Associate Editor of the IEEE TRANSACTIONS ON COMMUNICATIONS, the IEEE TRANSACTIONS ON WIRELESS COMMUNICATIONS, IEEE COMMUNICATIONS LETTERS, and IEEE ACCESS. He served as a Guest Editor for a Special Issue on Optical Wireless Communications of IEEE JOURNAL ON SELECTED AREAS IN COMMUNICATIONS. He is also a Registered Professional Engineer with the Province of British Columbia, Canada. He currently serves as the President of the Canadian Society of Information Theory as well as the Secretary for the Radio Communications Technical Committee of IEEE Communications Society.

BO AI (Senior Member, IEEE) received the master's and Ph.D. degrees from Xidian University, China.

He graduated from Tsinghua University with the honor of Excellent Postdoctoral Research Fellow with Tsinghua University in 2007. He was a Visiting Professor with the EE Department, Stanford University in 2015. He is currently working with Beijing Jiaotong University as a Full Professor and a Ph.D. Candidate Advisor. He is the Deputy Director of the State Key Laboratory of Rail Traffic Control and Safety, and the Deputy Director of the International Joint Research Center. He is one of the main responsible people for Beijing "Urban rail operation control system" International Science and Technology Cooperation Base, and the backbone member of the Innovative Engineering Based jointly granted by the Chinese Ministry of Education and the State Administration of Foreign Experts Affairs. He has hold 26 invention patents. He has been the research team leader for 26 national projects and has won some important scientific research prizes. Five papers have been the ESI highly cited. He has been notified by the Council of Canadian Academies that, based on the Scopus database, he has been listed as one of the top 1% of authors in his field. He has also been feature interviewed by *IET Electronics Letters*. His interests include the research and applications of channel measurement and channel modeling, dedicated mobile communications for rail traffic systems. He has authored/coauthored 8 books and published over 300 academic research papers in his research areas.

Prof. Ai has received many awards, such as the Distinguished Youth Foundation and Excellent Youth Foundation from National Natural Science Foundation of China, the Qiushi Outstanding Youth Award by Hong Kong Qiushi Foundation, the New Century Talents by the Chinese Ministry of Education, the Zhan Tianyou Railway Science and Technology Award by the Chinese Ministry of Railways, and the Science and Technology New Star by the Beijing Municipal Science and Technology Commission. He was a Co-Chair or a Session/Track Chair for many international conferences. He is an Associate Editor of IEEE ANTENNAS AND WIRELESS PROPAGATION LETTERS and the IEEE TRANSACTIONS ON CONSUMER ELECTRONICS, and an Editorial Committee Member of *Wireless Personal Communications*. He is the Lead Guest Editor for Special Issues on the IEEE TRANSACTIONS ON VEHICULAR TECHNOLOGY, IEEE ANTENNAS AND PROPAGATIONS LETTERS, and the *International Journal on Antennas and Propagations*. He is a Fellow of the Institution of Engineering and Technology and an IEEE VTS Distinguished Lecturer. He is an IEEE VTS Beijing Chapter Vice Chair and an IEEE BTS Xi'an Chapter Chair.